Molecular Cell

Article

PAICS ubiquitination recruits UBAP2 to trigger phase separation for purinosome assembly

Graphical abstract

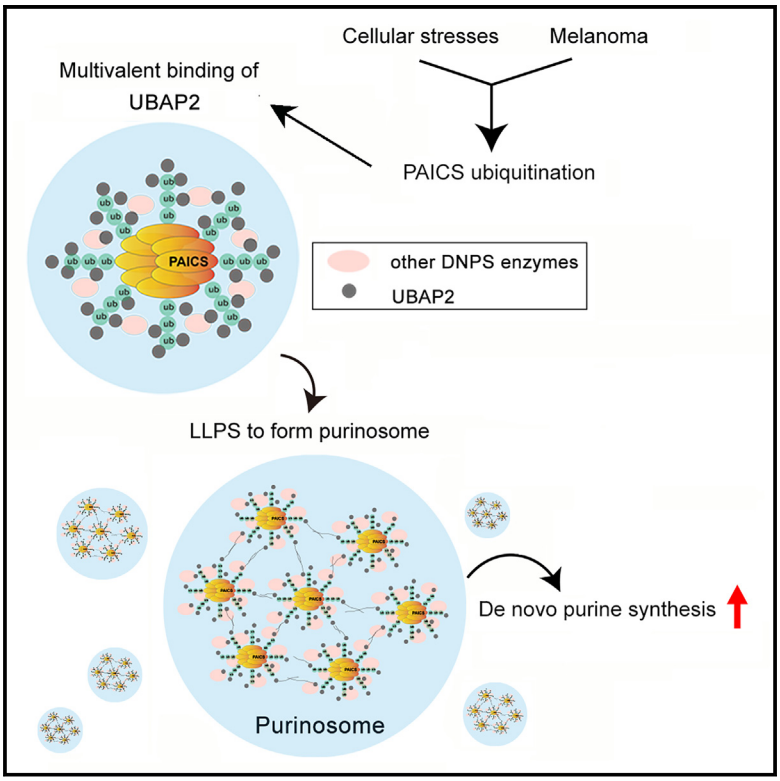

Highlights

- Stresses that increase purine demand upregulate ASB11 by epigenetic mechanisms
- ASB11 promotes PAICS ubiquitination to recruit the ubiquitin-binding protein UBAP2
- UBAP2 governs multivalent interactions to drive purinosome assembly
- Melanoma cells form purinosome constitutively to support their proliferation and survival

Authors

Ming-Chieh Chou, Yi-Hsuan Wang, Fei-Yun Chen, ..., Steven Firestine, Jie-rong Huang, Ruey-Hwa Chen

Correspondence

rhchen@gate.sinica.edu.tw

In brief

In this study, Chou et al. discovered that PAICS polyubiquitination induced by cell stresses triggers the recruitment of UBAP2 to confer multivalent interactions for driving phase separation to form purinosome condensates. Melanoma cells are addicted to the constitutive purinosome formation to supply sufficient purines for their proliferation and survival.

Chou et al., 2023, Molecular Cell *83*, 1–18
November 16, 2023 © 2023 Elsevier Inc.
https://doi.org/10.1016/j.molcel.2023.09.028

CellPress

Please cite this article in press as: Chou et al., PAICS ubiquitination recruits UBAP2 to trigger phase separation for purinosome assembly, Molecular Cell (2023), https://doi.org/10.1016/j.molcel.2023.09.028

Molecular Cell

CellPress

Article

PAICS ubiquitination recruits UBAP2 to trigger phase separation for purinosome assembly

Ming-Chieh Chou,[1,2,10] Yi-Hsuan Wang,[1,2,10] Fei-Yun Chen,[1] Chun-Ying Kung,[1,2] Kuen-Phon Wu,[1,2] Jean-Cheng Kuo,[3] Shu-Jou Chan,[1] Mei-Ling Cheng,[4,5,6] Chih-Yu Lin,[7] Yu-Chi Chou,[8] Meng-Chiao Ho,[1,2] Steven Firestine,[9] Jie-rong Huang,[3] and Ruey-Hwa Chen[1,2,11,*]

[1]Institute of Biological Chemistry, Academia Sinica, Taipei 115, Taiwan
[2]Institute of Biochemical Sciences, College of Life Science, National Taiwan University, Taipei 106, Taiwan
[3]Institute of Biochemistry and Molecular Biology, National Yang Ming Chiao Tung University, Taipei 112, Taiwan
[4]Metabolomics Core Laboratory, Healthy Aging Research Center, Chang Gung University, Taoyuan 333, Taiwan
[5]Graduate Institute of Biomedical Sciences, College of Medicine, Chang Gung University, Taoyuan 333, Taiwan
[6]Clinical Metabolomics Core Laboratory, Chang Gung Memorial Hospital at Linkou, Taoyuan 333, Taiwan
[7]Agricultural Biotechnology Research Center, Academia Sinica, Taipei 115, Taiwan
[8]Biomedical Translation Research Center, Academia Sinica, Taipei 115, Taiwan
[9]Department of Pharmaceutical Sciences, Eugene Applebaum College of Pharmacy and Health Sciences, Wayne State University, Detroit, MI 48201, USA
[10]These authors contributed equally
[11]Lead contact
*Correspondence: rhchen@gate.sinica.edu.tw
https://doi.org/10.1016/j.molcel.2023.09.028

SUMMARY

Purinosomes serve as metabolons to enhance *de novo* purine synthesis (DNPS) efficiency through compartmentalizing DNPS enzymes during stressed conditions. However, the mechanism underpinning purinosome assembly and its pathophysiological functions remains elusive. Here, we show that K6-polyubiquitination of the DNPS enzyme phosphoribosylaminoimidazole carboxylase and phosphoribosylaminoimidazolesuccinocarboxamide synthetase (PAICS) by cullin-5/ankyrin repeat and SOCS box containing 11 (Cul5/ASB11)-based ubiquitin ligase plays a driving role in purinosome assembly. Upon several purinosome-inducing cues, ASB11 is upregulated by relieving the H3K9me3/HP1α-mediated transcriptional silencing, thus stimulating PAICS polyubiquitination. The polyubiquitinated PAICS recruits ubiquitin-associated protein 2 (UBAP2), a ubiquitin-binding protein with multiple stretches of intrinsically disordered regions, thereby inducing phase separation to trigger purinosome assembly for enhancing DNPS pathway flux. In human melanoma, ASB11 is highly expressed to facilitate a constitutive purinosome formation to which melanoma cells are addicted for supporting their proliferation, viability, and tumorigenesis in a xenograft model. Our study identifies a driving mechanism for purinosome assembly in response to cellular stresses and uncovers the impact of purinosome formation on human malignancies.

INTRODUCTION

In metabolic pathway, the compartmentalization of sequential metabolic enzymes to form a non-covalent, supramolecular complex is termed metabolon, which is thought to enhance pathway flux through a substrate channeling effect.[1,2] Purinosomes represent one type of metabolons and consist of all six enzymes in the *de novo* purine synthesis (DNPS) pathway, together with other enzymes, contributing to purine synthesis.[3–6] The formation of purinosomes in cytoplasm is induced by purine-depleted medium (PDM), inhibition of oxidative phosphorylation (OXOPHOS), or signaling cues, including G protein-coupled receptor (GPCR) agonist and casein kinase 2 (CK2) inhibitors.[3,7–10] A recent study provides direct evidence for the metabolite channeling effect conferred by purinosome assembly.[11] However, the mechanism driving purinosome assembly remains poorly understood. Interestingly, interactions among DNPS enzymes are detected even under purine-rich medium.[4] Furthermore, purinosomes possess several features of liquid-like condensates.[12,13] These findings imply that a liquid-liquid phase separation (LLPS) process triggers the coalescence of pre-existing DNPS enzyme complexes into larger, microscopically visible granules, a mechanism analogous to that of stress granule assembly.[14] However, the nature of such LLPS event remains completely unexplored.

DNPS is often utilized by cells with a high demand on purines, such as tumor cells.[15] Accordingly, the activity and expression of

Please cite this article in press as: Chou et al., PAICS ubiquitination recruits UBAP2 to trigger phase separation for purinosome assembly, Molecular Cell (2023), https://doi.org/10.1016/j.molcel.2023.09.028

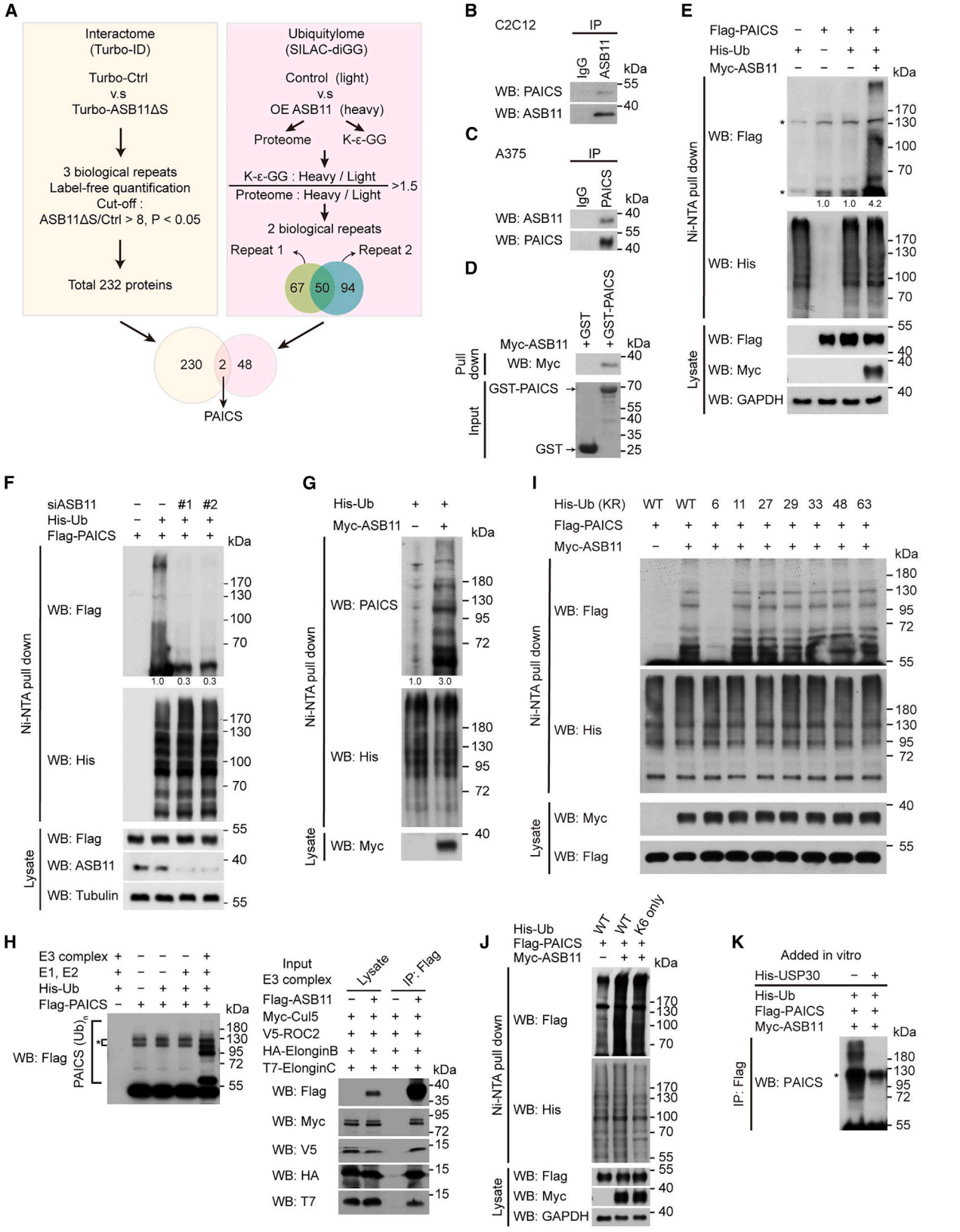

(legend on next page)

Please cite this article in press as: Chou et al., PAICS ubiquitination recruits UBAP2 to trigger phase separation for purinosome assembly, Molecular Cell (2023), https://doi.org/10.1016/j.molcel.2023.09.028

DNPS enzymes are dysregulated in various cancer types,[16] and elevated DNPS is linked to several malignant hallmarks, including proliferation, cancer stemness, metastasis, and therapy resistance.[17–20] By functioning as a metabolon, purinosome may elicit certain pro-tumor effects, such as the stimulation of purine production to fuel tumor cells. However, such idea has not been validated.

Phase separation, a process by which a homogeneous solution demixes to form a dense and dilute phase, is a prime mechanism for the assembly of membraneless biomolecular condensates.[21–23] Accumulating evidence indicates that multivalent interaction serves as a driving force for phase separation, and such interaction is often mediated by proteins containing intrinsically disordered regions (IDRs) and/or multiple-folded modular domains.[24–26] Phase separation is tightly regulated in the intracellular environment through multiple mechanisms and protein posttranslational modifications, including ubiquitination, are among the major mechanisms.[27,28] Ubiquitin (Ub) exerts positive or negative impacts on phase separation. For instance, Ub binding to certain Ub-binding proteins (UBPs) results in the disruption of pre-existing multivalent interactions, as seen in the disassembly of stress granules and UBQLN2 condensates.[29,30] In contrast, the multivalent binding between polyubiquitin (polyUb) chain and UBP could directly induce phase separation. To date, a number of polyUb-based phase separation events have been reported to function in diverse cellular processes, including polyUb binding to p62 for selective autophagy,[31–33] to RAD23B for stress-induced proteasome foci formation,[34] to NFκB essential modulator (NEMO) for activating nuclear factor κB (NF-κB) signaling,[35,36] and to endosomal sorting complexes required for transport (ESCRT)-0 for endocytic cargo sorting.[37] Intriguingly, different polyUb chains can enhance or inhibit UBQLN2 phase separation, depending on the chain conformation.[38] Furthermore, ubiquitination of dishevelled segment polarity protein 2 (Dvl2), an IDRs-containing protein capable of oligomerization, directly triggers phase separation without the involvement of UBP.[39]

In this study, we identify a key role of DNPS enzyme PAICS ubiquitination in driving purinosome assembly through LLPS. In response to several purinosome-inducing cues, ASB11, a substrate adaptor of Cul5 Ub ligase,[40,41] is upregulated through epigenetic mechanisms, thereby promoting K6-linked polyubiquitination on PAICS. The polyubiquitinated PAICS recruits UBAP2, a protein containing a UBA domain and multiple IDRs, to trigger purinosome assembly. We further uncover a constitutive purinosome formation in melanoma and its importance in melanoma malignant progression.

RESULTS

PAICS is a substrate of ASB11-based Ub ligase

To systematically identify the substrates of ASB11-based Ub ligase, we undertook an unbiased approach by combining interactome and ubiquitylome analyses. For interactome analysis, we used a proximity labeling approach by transfecting TurboID-tagged ASB11ΔS (suppressors of cytokine signaling [SOCS] box deletion) to 293T cells, as this mutant likely functions as a substrate trap due to inability to assemble the Cul5 complex.[40,41] The biotinylated proteins were purified and analyzed by liquid chromatography-tandem mass spectrometry (LC-MS/MS), and a total of 232 proteins were identified as ASB11-interacting proteins (Figure 1A; Table S1). For ubiquitylome analysis, control and ASB11-overexpressing 293T cells were labeled with stable-isotope labeling by amino acids in cell culture (SILAC) and subjected to LC-MS/MS for detecting ubiquitylome and proteome changes. For the former, we used immunoprecipitation with K-ε-GG antibody to enrich ubiquitinated peptides.[42] By normalizing Ub level changes with protein level changes, we uncovered 50 proteins showing elevated ubiquitination by ASB11 overexpression (Figure 1A; Table S2). Importantly, the DNPS enzyme PAICS was identified from both interactome and ubiquitylome analyses (Figure 1A).

Validation experiments showed that ASB11 and PAICS interacted in transfected cells and endogenously in C2C12 and A375 cells (Figures 1B, 1C, and S1A). GST pull-down analysis detected the interaction between bacterially purified PAICS and ASB11 from cell lysates (Figure 1D). Remarkably, the ubiquitination level of PAICS was increased by overexpression of ASB11 but not of ASB11ΔS (Figures 1E and S1B). Conversely, ASB11 knockdown (KD) diminished PAICS ubiquitination (Figure 1F). ASB11 was also capable of potentiating the ubiquitination of endogenous PAICS (Figure 1G). Finally, *in vitro* ubiquitination assay demonstrated that purified PAICS was ubiquitinated by purified $Cul5^{ASB11}$ E3 ligase complex (Figure 1H). Our data thus identify PAICS as a substrate of ASB11-based Ub ligase.

ASB11 promotes a non-degradable, K6-polyubiquitination on PAICS

Despite being a substrate of ASB11-based Ub ligase, PAICS abundance was not affected by ASB11 overexpression or KD (Figures S1C–S1E). PAICS was stabilized by cycloheximide treatment for 24 h and remained stable in ASB11-overexpressing or KD cells (Figures S1F and S1G). Cycloheximide treatment also did not affect the level of ubiquitinated PAICS (Figure S1H). These findings point to a non-degradable fate of ASB11-mediated

Figure 1. ASB11 promotes a K6-linked polyubiquitination on PAICS

(A) Schematic of ASB11 interactome and ASB11-altered ubiquitylome analyses.

(B and C) PAICS-ASB11 interaction in C2C12 and A375 cells.

(D) *In vitro* binding assay with GST-PAICS from bacteria and Myc-ASB11 from transfected 293T cells.

(E and F) PAICS ubiquitination in 293T cells transfected with indicated constructs. Asterisks denote non-specific bands.

(G) Endogenous PAICS ubiquitination in 293T cells transfected with indicated constructs.

(H) *In vitro* ubiquitination assay for PAICS. Asterisk denotes non-specific bands. The integrity of input E3 ligase complex is shown.

(I and J) PAICS ubiquitination in 293T cells transfected with indicated constructs.

(K) PAICS immunoprecipitated from transfected 293T cells was treated with USP30, followed by western blot analysis of PAICS ubiquitination. Asterisk denotes a non-specific band. See also Figures S1 and S2 and Tables S1 and S2.

Please cite this article in press as: Chou et al., PAICS ubiquitination recruits UBAP2 to trigger phase separation for purinosome assembly, Molecular Cell (2023), https://doi.org/10.1016/j.molcel.2023.09.028

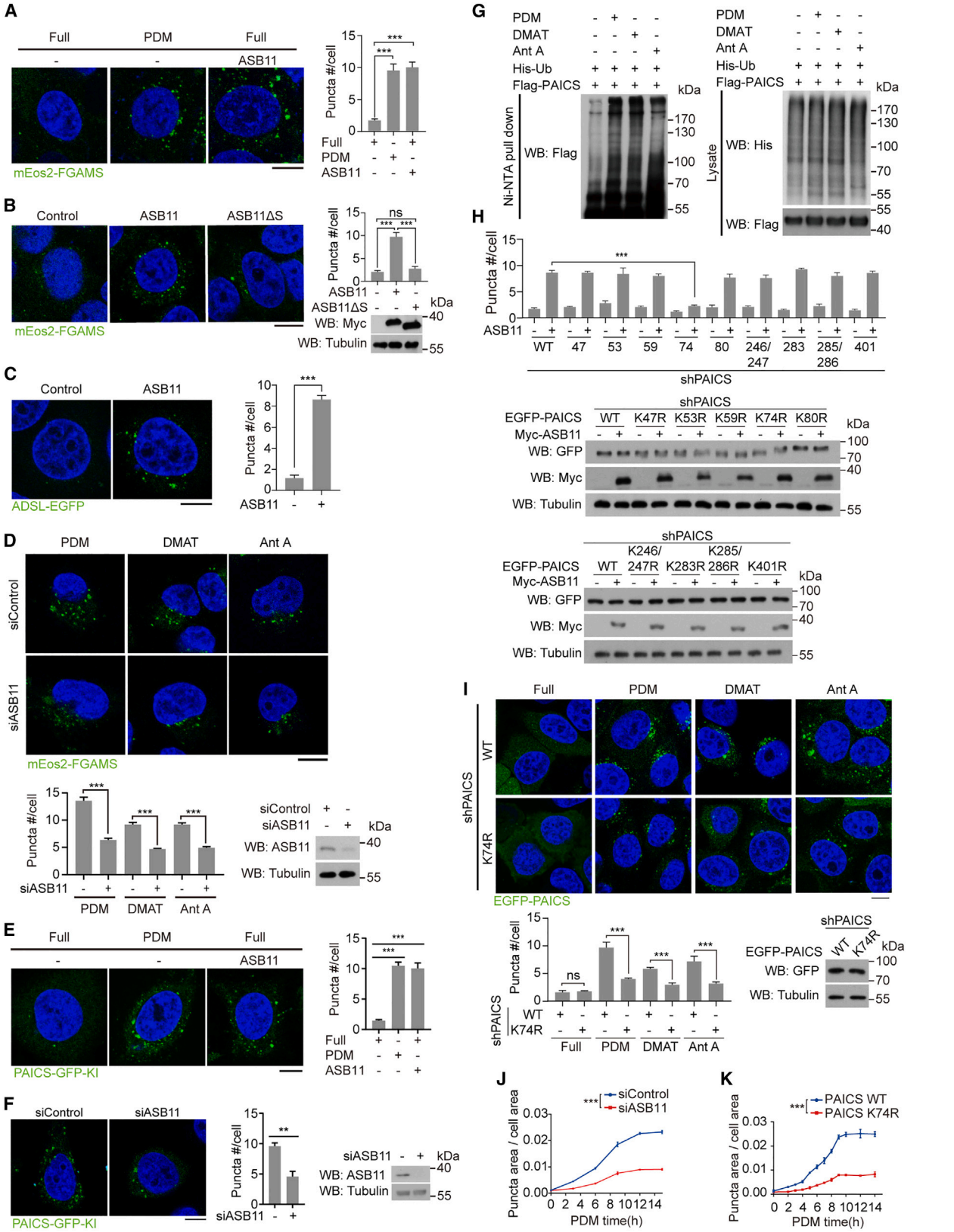

(legend on next page)

Please cite this article in press as: Chou et al., PAICS ubiquitination recruits UBAP2 to trigger phase separation for purinosome assembly, Molecular Cell (2023), https://doi.org/10.1016/j.molcel.2023.09.028

PAICS ubiquitination. We thus analyzed the polyUb chain type on PAICS. Intriguingly, K48- and K63-polyubiquitinations of PAICS were decreased by ASB11 overexpression (Figure S1I), presumably due to the competition with other polyUb chain types. Using a panel of Ub KR mutants to disrupt the formation of each polyUb chain, we found that only the K6R Ub could not support ASB11-mediated PAICS polyubiquitination (Figure 1I). Furthermore, the K6-only Ub could confer ASB11-induced PAICS ubiquitination as the wild-type (WT) Ub (Figure 1J). Treatment of PAICS immunoprecipitated from ASB11/His-Ub-overexpressing cells with ubiquitin-specific protease 30 (USP30), a deubiquitinase selectively hydrolyzing the K6-polyUb chain,[43] abrogated PAICS polyubiquitination (Figure 1K). To identify the ubiquitinated residues on PAICS in ASB11-overexpressing cells, we treated the immunoprecipitated PAICS with Lb* protease, which removes all Ub moieties from substrate to leave Gly-Gly at the modified Lys residue.[44] The cleaved substrate was excised from gel for LC-MS/MS analysis (Figure S2A). This method reduced sample complexity to enhance the detection of modified Lys. We identified a set of ubiquitinated residues on PAICS (Figure S2B). Mutational analysis revealed a reduced ubiquitination signal by K74R mutation, whereas other mutations had little effect (Figure S2C). Thus, our study supports that ASB11 mediates a non-degradable K6-polyubiquitination on PAICS and that K74 residue of PAICS is the major ubiquitination site targeted by ASB11.

ASB11-mediated PAICS polyubiquitination drives purinosome assembly

Next, we determined the consequence of ASB11-mediated PAICS ubiquitination. Using purinosome marker mEos2-phosphoribosyl formylglycinamidine synthase (FGAMS), we found that ASB11 overexpression induced purinosome formation without the need of PDM treatment, and this effect of ASB11 overexpression resembled PDM treatment (Figures 2A and S3A). ASB11ΔS mutant failed to induce purinosomes (Figure 2B), suggesting the involvement of E3 ligase function. To substantiate the identity of mEos2-FGAMS puncta as purinosomes, we used another purinosome marker adenylosuccinate lyase (ADSL)-EGFP and a dual marker strategy by co-expressing mEos2-FGAMS and mCherry-PAICS.[3] ASB11 overexpression increased ADSL-EGFP puncta and mEos2-FGAMS/mCherry-PAICS double-positive puncta (Figures 2C and S3B). In the reciprocal experiment, ASB11 depletion reduced purinosome numbers in cells treated with several purinosome-inducing agents, including PDM, 2-dimethylamino-4,5,6,7-tetrabromo-1H-benzimidazole (DMAT, a CK2 inhibitor), and antimycin A (OXOPHOS inhibitor) (Figure 2D). Furthermore, this effect of ASB11 depletion on the reduction of purinosome formation was rescued by re-expressing WT ASB11 but not ASB11ΔS (Figure S3C). Interestingly, ASB11 not only promoted purinosome assembly but was itself recruited to purinosomes (Figure S3D). Our findings identify the critical role of ASB11 in purinosome assembly.

Since purinosome is disrupted by detergents used for cell permeabilization during immunostaining, previous studies relied on overexpression of fluorescently tagged DNPS enzymes for purinosome detection.[5] To visualize purinosomes at the endogenous levels, we adopt the split-GFP strategy[45] by introducing the 11th β strand of GFP (GFP_{11}) to the C terminus of PAICS in the genome of HeLa cells via CRISPR-Cas9 technology. The resulting cells were transfected with the remainder of superfolder GFP ($GFP_{1–10}$) to reconstitute an intact GFP, thus enabling GFP tagging of endogenous PAICS. With this strategy, we observed a remarkable co-localization of mCherry-FGAMS puncta with the PAICS-GFP-knockin (KI) puncta in PDM-treated cells and a great induction of PAICS-GFP-KI puncta by multiple purinosome-inducing cues (Figures 2E, S3E, and S3F), thus supporting the PAICS-GFP-KI puncta as *bona fide* purinosomes. Moreover, ASB11 overexpression in this split-GFP system stimulated endogenous purinosome assembly, and an opposite effect was observed by ASB11 KD under PDM treatment (Figures 2E and 2F). Our study not only establishes a method to monitor purinosomes at the endogenous levels but substantiates the critical role of ASB11 in purinosome assembly.

Next, we determined whether the effect of ASB11 on purinosome assembly is attributed to PAICS ubiquitination. We first observed an enrichment of Ub signal in purinosomes and an upregulation of PAICS ubiquitination by various purinosome-inducing cues (Figures 2G and S3G). To provide direct evidence for the role of PAICS ubiquitination in purinosome assembly, we reconstituted PAICS ubiquitination site mutants to PAICS KD cells. PAICS K74R mutation, but not all other mutations, compromised purinosome formation induced by ASB11 overexpression (Figures 2H and S3H), consistent with a major role of this residue

Figure 2. ASB11-mediated PAICS ubiquitination drives purinosome assembly

(A–C) Purinosome formation in HeLa cells transfected with indicated purinosome markers and ASB11 or mutant and cultured in full medium or PDM. The expression levels of ASB11 and mutant are shown.

(D) Purinosome formation in A375 cells transfected with mEos2-FGAMS and ASB11 small interfering RNA (siRNA) and treated with indicated agents. The knockdown efficiency of ASB11 siRNA is shown.

(E and F) Endogenous purinosome formation in HeLa GFP_{11} knockin cells transfected with $GFP_{1–10}$, together with ASB11 or ASB11 siRNA, and/or treated with PDM. The knockdown efficiency of ASB11 siRNA is shown.

(G) PAICS ubiquitination in 293T cells transfected with indicated constructs and treated with indicated agents.

(H) Purinosome numbers in HeLa-sh (short hairpin) PAICS cells transfected with EGFP-PAICS or mutants, together with ASB11. Representative confocal images are shown in Figure S3H. The expression levels of various EGFP-PAICS mutants are shown.

(I) Purinosome formation in HeLa-shPAICS cells transfected with EGFP-PAICS WT or K74R and treated with indicated agents. The expression levels of EGFP-PAICS and mutant are shown.

(J and K) Kinetics of purinosome formation in HeLa cells (J) or HeLa-shPAICS cells (K) transfected with mEos2-FGAMS and indicated constructs and treated with PDM for indicated times. Quantitative data in all panels are mean ± SD; n = 3, $^{**}p < 0.01$ and $^{***}p < 0.001$ by one-way ANOVA with Tukey's multiple comparisons test (A–C and E), two-way ANOVA with Sidak's multiple comparisons test (D, H, and I), unpaired t test (F), or two-way repeated measures ANOVA test (J and K); ns, not significant. Scale bars, 10 μm. See also Figure S3.

Please cite this article in press as: Chou et al., PAICS ubiquitination recruits UBAP2 to trigger phase separation for purinosome assembly, Molecular Cell (2023), https://doi.org/10.1016/j.molcel.2023.09.028

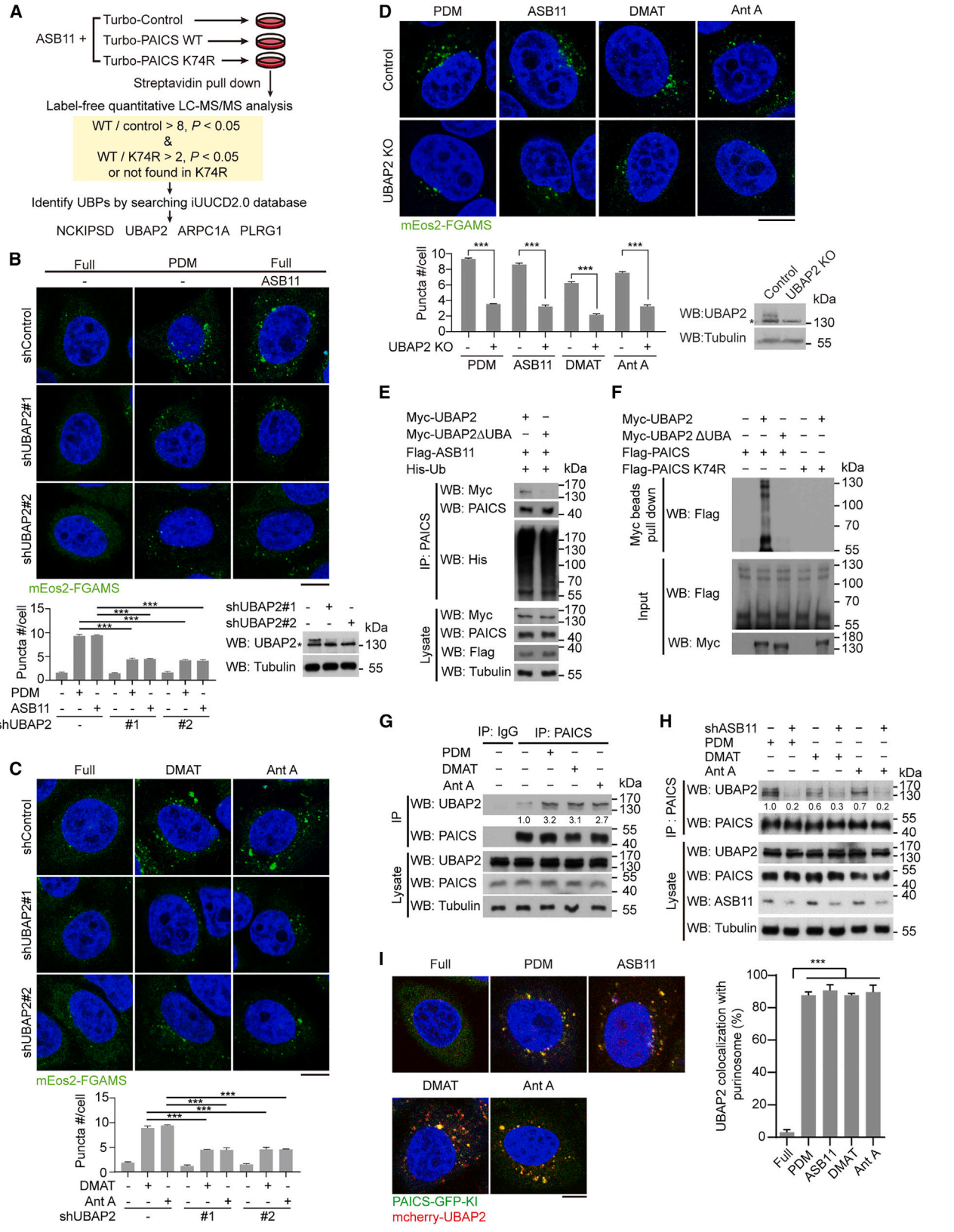

(legend on next page)

Please cite this article in press as: Chou et al., PAICS ubiquitination recruits UBAP2 to trigger phase separation for purinosome assembly, Molecular Cell (2023), https://doi.org/10.1016/j.molcel.2023.09.028

in conferring ASB11-mediated PAICS ubiquitination (Figure S2C). PAICS K74R mutation also impaired purinosome induction by PDM, DMAT, or antimycin A (Figure 2I). Intriguingly, PAICS K74R mutation or ASB11 depletion decreased purinosome formation efficiency without affecting the timing of purinosome induction (Figures 2J and 2K). Notably, purinosome-inducing cues did not affect the expression of any DNPS enzyme (Figure S3I). These data reveal a key role of PAICS K74 ubiquitination by ASB11 in driving purinosome assembly.

The K74 residue is located in the succinylaminoimidazolecarboxamide ribose-5′-phosphate (SAICAR) synthetase (SAICARs) domain of PAICS, away from the active site (Figure S3J). Importantly, K74R mutation altered neither the SAICARs enzymatic activity of PAICS nor PAICS 3D architecture, as assayed by ADP generation from 4-carboxy-5-aminoimidazole ribonucleotide (CAIR) and L-aspartate and circular dichroism (CD), respectively (Figures S3K and S3L), thus excluding the possibility for a reduced enzymatic activity to impede purinosome formation.

Ubiquitinated PAICS recruits UBAP2 to drive purinosome assembly

How does PAICS K74 ubiquitination drive purinosome assembly? Since PAICS forms an octamer,[46] the octameric and polyubiquitinated PAICS may recruit a UBP to confer multivalent interactions, thereby triggering LLPS to drive purinosome assembly. To identify such UBP, we employed TurboID-based proximity labeling assay to identify proteins that bind preferentially to PAICS over PAICS K74R in cells overexpressing ASB11 (Figure 3A). Among the hits uncovered (Table S3), we searched for UBPs by querying the iUUCD2.0 database http://iuucd.biocuckoo.org/[47] and identified four potential UBPs. KD experiments showed that only UBAP2, but not other UBPs, was critical for purinosome formation in ASB11-overexpressing cells (Figures 3B and S4A). UBAP2 silencing also compromised purinosome formation induced by PDM, DMAT, or antimycin A (Figures 3B and 3C). Similarly, UBAP2 knockout (KO) by CRISPR impaired purinosome formation under ASB11 overexpression or other purinosome-inducing conditions (Figure 3D). Furthermore, endogenous purinosome formation was suppressed by UBAP2 KD (Figure S4B). Similar to PAICS K74R mutation and ASB11 depletion, UBAP2 KO decreased purinosome formation efficiency without affecting the timing of purinosome induction (Figure S4C). These findings identify a critical role of UBAP2 in purinosome assembly.

UBAP2 contains a UBA domain. We determined whether this domain mediates the interaction between UBAP2 and polyubiquitinated PAICS. In cells overexpressing ASB11 and His-Ub to boost PAICS ubiquitination, we detected not only endogenous PAICS polyubiquitination but also PAICS interaction with UBAP2 but not UBAP2ΔUBA (Figure 3E). We further analyzed the binding between ubiquitinated PAICS and UBAP2 *in vitro*, in which UBAP2 was purified from baculovirus, whereas PAICS was immunoprecipitated from ASB11/Ub-transfected 293T cells. Importantly, UBAP2, but not UBAP2ΔUBA, bound on Myc-beads could readily pull down ubiquitinated PAICS, whereas PAICS K74R mutant did not interact with UBAP2 (Figure 3F). Furthermore, treatment of ubiquitinated PAICS with USP30 not only disassembled polyUb chain on PAICS but also compromised PAICS interaction with UBAP2 (Figure S4D). Thus, the interaction of UBAP2 with PAICS requires the UBA domain of UBAP2 and the polyubiquitination at K74 residue of PAICS.

Notably, various purinosome-inducing cues, including PDM, DMAT, and antimycin A, increased the interaction between endogenous UBAP2 and endogenous PAICS, which was reversed by ASB11 depletion (Figures 3G and 3H). These findings support the idea that ASB11-mediated PAICS ubiquitination recruits UBAP2 to PAICS under purinosome-inducing conditions. In normal culturing conditions, UBAP2 was dispersedly located in the cytoplasm in a majority of cells, and only a small population of cells exhibited the localization of UBAP2 to large cytoplasmic puncta (Figure S4E). The large size and the lack of co-localization with purinosome marker excluded their identity as purinosomes. In response to various purinosome-inducing cues however, UBAP2 was relocated to purinosomes and co-localized with mEos2-FGAMS or PAICS-GFP-KI puncta (Figures 3I and S4E). Proximity ligation assay (PLA) revealed increased interactions of UBAP2 with DNPS enzymes, such as PAICS and ADSL, by PDM treatment or ASB11 overexpression (Figures S4F and S4G). Our data support the hypothesis that induction of PAICS polyubiquitination by purinosome-inducing cues leads to UBAP2 recruitment to drive purinosome assembly. Consequently, UBAP2 is co-localized with DNPS enzymes in purinosomes.

Binding polyUb and carrying IDRs are both required for UBAP2 to trigger LLPS and purinosome assembly

Apart from the UBA domain, UBAP2 contains eight stretches of IDRs located throughout its primary sequence, as predicted by

Figure 3. Ubiquitinated PAICS recruits UBAP2 to drive purinosome assembly

(A) Schematic of the strategies for UBPs identification.

(B and C) Purinosome formation in HeLa or HeLa-shUBAP2 cells transfected with mEos2-FGAMS and ASB11 and/or treated with indicated agents. The knockdown efficiencies of UBAP2 short hairpin RNAs (shRNAs) are shown in (B). Asterisk denotes a non-specific band.

(D) Purinosome formation in HeLa UBAP2 KO cells transfected with mEos2-FGAMS and ASB11 and treated with indicated agents. UBAP2 KO was verified by western blot. Asterisk denotes a non-specific band.

(E) UBAP2 or UBAP2ΔUBA interaction with PAICS in HeLa-shUBAP2 cells transfected with UBAP2 or mutant, together with ASB11 and His-Ub.

(F) *In vitro* binding between Myc-UBAP2 purified from baculovirus and ubiquitinated FLAG-PAICS or mutants purified from transfected cells.

(G and H) PAICS-UBAP2 interaction in HeLa cells treated with indicated agents (G) or A375 cells stably expressing isopropyl β-D-1-thiogalactopyranoside (IPTG)-inducible ASB11 shRNA, treated with 0.5 μM IPTG for 5 days, and treated with indicated agents (H).

(I) Co-localization of mCherry-UBAP2 with endogenous purinosomes in HeLa GFP_{11} knockin cells transfected with $GFP_{1–10}$ and mCherry-UBAP2 together with ASB11 and/or treated with indicated agents. Quantitative data in all panels are mean ± SD (n = 3), ***$p < 0.001$ by two-way ANOVA with Dunnett's multiple comparisons test (B and C), two-way ANOVA with Sidak's multiple comparisons test (D), or one-way ANOVA with Dunnett's multiple comparisons test (I). Scale bars, 10 μm. See also Figure S4 and Table S3.

Please cite this article in press as: Chou et al., PAICS ubiquitination recruits UBAP2 to trigger phase separation for purinosome assembly, Molecular Cell (2023), https://doi.org/10.1016/j.molcel.2023.09.028

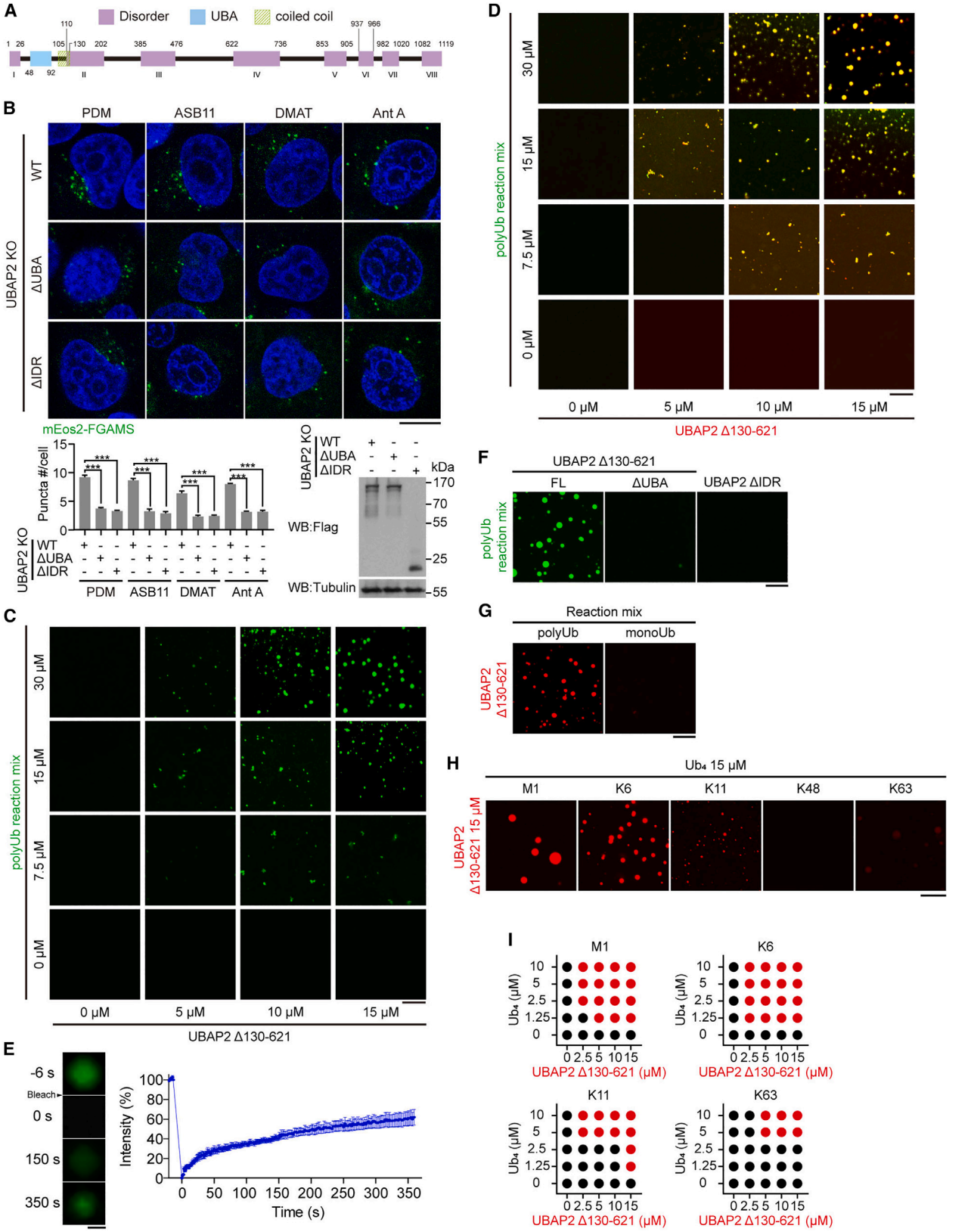

(legend on next page)

Please cite this article in press as: Chou et al., PAICS ubiquitination recruits UBAP2 to trigger phase separation for purinosome assembly, Molecular Cell (2023), https://doi.org/10.1016/j.molcel.2023.09.028

MobiDB-lite from the MobiDB (https://mobidb.bio.unipd.it/) (Figure 4A). Consistently, *in silico* structural prediction by AlphaFold (https://alphafold.ebi.ac.uk/) revealed that the region outside the UBA domain is mainly unstructured (Figure S5A). To determine the contributions of UBA domain and IDRs to purinosome formation, we reconstituted UBAP2 WT, ΔUBA mutant (Δ48–92), or ΔIDR mutant (Δ130–1,119) to UBAP2 KO cells. Consistent with its inability to bind ubiquitinated PAICS, ΔUBA mutant could not rescue purinosome formation in response to various purinosome-inducing cues. However, ΔIDR mutant similarly could not support purinosome formation, in sharp contrast to UBAP2 WT (Figure 4B). To evaluate the contributions of different stretches of IDRs, we generated a panel of mutants to delete them individually or in combination, except for the shortest IDR I. We found that deletion of IDR IV (Δ622–736), IDR V–VI (Δ853–966), or IDR VII–VIII (Δ982–1,119) decreased purinosome numbers to a certain extent, whereas IDR II deletion (Δ130–202) did not show a significant effect (Figure S5B). IDR III deletion (Δ385–476) mutant could not be expressed, thus precluding an evaluation. Additionally, replacement of the UBAP2 UBA domain with the UBA domain of USP5 (termed UBAP2 UBA^R mutant) did not affect purinosome formation induced by various cues (Figure S5C). Our study reveals that UBA and IDRs are both required for UBAP2 to drive purinosome formation, and contribution of the latter is shared by at least several C-terminal IDRs.

Previous studies found that purinosomes resemble liquid-like condensates.[12,13] Accordingly, real-time confocal analysis revealed that the mEos2-FGAMS droplets seen in ASB11-overexpressing cells were highly dynamic, and droplet fusion event was readily observed (Figure S5D). Furthermore, fluorescence recovery after photobleaching (FRAP) analysis showed a partial but rapid recovery of mEos2-FGAMS signal in purinosomes present in ASB11-overexpressing cells (Figure S5E). Similarly, both mCherry-UBAP2 and PAICS-GFP-KI signals were recovered rapidly after photobleaching of endogenous purinosomes, and the fusion of endogenous purinosomes was observed (Figures S5F and S5G). Thus, endogenous purinosomes and purinosomes formed by an ASB11-dependent mechanism also possess features of liquid-like condensates.

Data described above support a model that recruitment of UBAP2 by polyubiquitinated PAICS drives purinosome assembly through LLPS. We therefore tested whether the K6-linked polyUb chain could induce LLPS of UBAP2 *in vitro*. To generate K6-linked polyUb, we undertook a previously established protocol[48] by using NleL E3 ligase together with Ub K48R (Figure S5H). As to UBAP2, we used Δ130–621 mutant because of the inability of expressing full-length UBAP2 in *E. coli* and the ability of this mutant to support purinosome formation as efficiently as UBAP2 WT (Figure S5B). Incubation of purified UBAP2Δ130–621 (Figure S5I) with fluorescein-5-maleimide (FM)-labeled polyUb in ubiquitination reaction mixture resulted in the formation of droplets, and droplet numbers and sizes were increased with the increased concentrations of polyUb and UBAP2Δ130–621 (Figure 4C). A similar result was observed by mixing FM-labeled polyUb with Alexa Fluor 647-labeled UBAP2Δ130–621 (Figure 4D). FRAP analysis revealed that the FM-polyUb signals in the condensates were rapidly recovered (Figure 4E). Furthermore, removal of UBA or IDRs abrogated condensate formation, whereas monoUb (without adding the NleL E3 ligase to reaction mix) was defective in supporting condensate formation by mixing with UBAP2Δ130–621 (Figures 4F, 4G, S5H, and S5I). To determine the capacity of different polyUb chain types to induce UBAP2 LLPS, we mixed Alexa Fluor 647-labeled UBAP2Δ130–621 with purified Ub_4, linked by M1, K6, K11, K48, or K63 chain. At high concentrations of both components, LLPS was detected with each Ub_4 except for K48-Ub_4 (Figures 4H and S5J). By sequentially reducing the concentrations of both components, we found that reactions with K6-Ub_4 exhibited the lowest threshold concentrations of Ub_4 and UBAP2Δ130–621 necessary for LLPS (Figure 4I). Biolayer interferometry analysis revealed modest differences in the binding affinity of these Ub_4 to the UBAP2 UBA domain (Figure S5K), but the affinity roughly correlated with the efficacy in promoting UBAP2Δ130–621 LLPS (comparing Figure S5K with Figure 4I). Thus, the K6-polyUb chain is capable of inducing UBAP2Δ130–621 LLPS *in vitro*, which requires the cooperation of polyUb (representing tandem folded domains)- and IDR (representing unstructured sequences)-mediated multivalency. Furthermore, different polyUb chains possess different capacities in driving UBAP2Δ130–621 LLPS.

Purinosome formation enhances DNPS pathway flux

Purinosome formation increases DNPS pathway flux in PDM-treated cells,[11] but whether a similar effect occurs in other

Figure 4. Binding polyUb and carrying IDRs are both required for UBAP2 to trigger LLPS and purinosome assembly

(A) UBAP2 domain architecture.

(B) Purinosome formation in HeLa UBAP2 KO cells reconstituted with UBAP2 WT or mutants and transfected with ASB11 or treated with indicated agents. Data are mean ± SD; n = 3, ***p < 0.001 by two-way ANOVA with Dunnett's multiple comparisons test. The expression levels of reconstituted UBAP2 and mutants are shown.

(C and D) *In vitro* phase separation assays by mixing indicated concentrations of unlabeled (C) or 1% Alexa Fluor 647-labeled (D) UBAP2Δ130–621 with increasing amounts of the ubiquitination reaction mix containing E1, E2 (UbcH7), E3 (NleL), and 1% FM-labeled Ub K48R. The concentrations indicated are Ub K48R input in the reaction mix.

(E) FRAP assay of droplets formed by LLPS assay as in (C). Data are mean ± SEM (n = 10).

(F and G) *In vitro* phase separation assay by mixing 15 μM unlabeled UBAP2 mutants with ubiquitination reaction mix containing 15 μM Ub K48R (1% FM-labeled) (F) or 15 μM UBAP2Δ130–621 (1% Alexa Fluor 647-labeled) with ubiquitination reaction mix containing 15 μM unlabeled Ub K48R with or without E3 (G).

(H) *In vitro* phase separation by mixing 15 μM UBAP2Δ130–621 (1% Alexa Fluor 647-labeled) with 15 μM Ub_4.

(I) Phase diagrams of reactions as in (H), with indicated concentrations of each component. Red and black circles represent LLPS positive and negative, respectively.

Scale bars, 1 μm (E) or 10 μm (other panels). For all LLPS experiments, the purity of input proteins and the formation of polyUb chain are shown in Figures S5H–S5J. See also Figure S5.

Please cite this article in press as: Chou et al., PAICS ubiquitination recruits UBAP2 to trigger phase separation for purinosome assembly, Molecular Cell (2023), https://doi.org/10.1016/j.molcel.2023.09.028

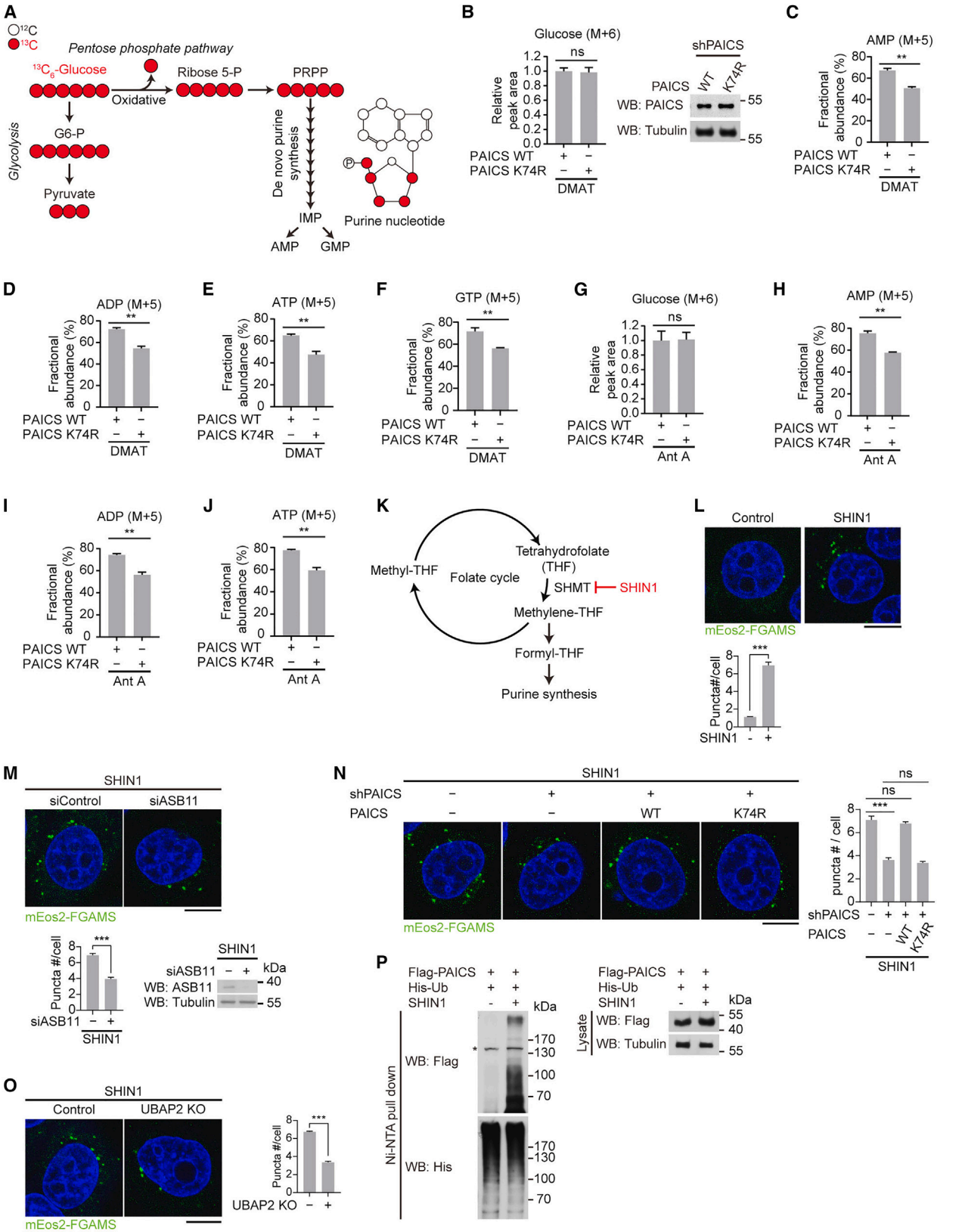

(legend on next page)

Please cite this article in press as: Chou et al., PAICS ubiquitination recruits UBAP2 to trigger phase separation for purinosome assembly, Molecular Cell (2023), https://doi.org/10.1016/j.molcel.2023.09.028

purinosome-inducing conditions remains uncharacterized. We thus performed metabolite tracing analysis on PAICS KD cells reconstituted with PAICS WT (purinosome-proficient) or PAICS K74R (purinosome-deficient) for measuring the relative flux of stable isotope-labeled $^{13}C_6$-glucose to purines (Figure 5A). The cells were treated with DMAT and then labeled with $^{13}C_6$-glucose. With a short-term labeling (5 min), the intracellular level of $^{13}C_6$-glucose was no different between PAICS WT and PAICS K74R cells (Figure 5B), suggesting an equal uptake of the tracer. However, under long-term labeling (14 h), the fractional abundances of labeled purine intermediates such as AMP, ADP, ATP, and GTP were all higher in PAICS WT cells compared with PAICS K74R cells (Figures 5C–5F). Similar findings were observed from antimycin A-treated cells (Figures 5G–5J). Thus, purinosome formation induced by DMAT or antimycin A enhances the flux of DNPS pathway.

Pharmacological inhibition of DNPS induces purinosome assembly through a PAICS-ubiquitination-dependent mechanism

While PDM limits extracellular purines to induce purinosome formation, it remains unclear whether decrease of intracellular purines by DNPS inhibition could similarly induce purinosomes through a PAICS-ubiquitination-dependent mechanism. The folate cycle enzyme serine hydroxymethyltransferase (SHMT) converts serine and tetrahydrofolate into glycine and 5,10-methylenetetrahydrofolate to contribute to DNPS (Figure 5K). Accordingly, inhibition of SHMT by a folate-competitive inhibitor SHIN1 (SHMT inhibitor 1) causes intracellular purine depletion.[49] We found that SHIN1 induced purinosome formation (Figure 5L). Furthermore, ASB11 depletion, replacement of PAICS WT with K74R, or UBAP2 KO each compromised purinosome formation induced by SHIN1 (Figures 5M–5O). SHIN1 also upregulated PAICS ubiquitination (Figure 5P). Thus, inhibition of DNPS by limiting substrate availability induces purinosome formation through a PAICS ubiquitination- and UBAP2-dependent mechanism.

Purinosome-inducing cues elevate ASB11 expression by suppressing H3K9m3/HP1α-mediated transcriptional silencing

Next, we investigated how PAICS ubiquitination is enhanced by purinosome-inducing cues. Strikingly, *ASB11* mRNA was upregulated by PDM, DMAT, or antimycin A treatment (Figures 6A and S6A), leading to increased ASB11 protein expression and ASB11-PAICS interaction (Figure S6B). SHIN1 also upregulated *ASB11* mRNA and protein (Figures 6B and S6C). Given the tight connection between metabolic reprogramming and epigenetic regulation,[50] we performed steady-state metabolic profiling analysis to interrogate whether metabolite-induced epigenetic regulation underlies *ASB11* upregulation by PDM. Remarkably, three of the four urea cycle metabolites were downregulated by PDM, accompanied with the decrease of urea cycle product fumarate (Figure 6C; Table S4). Since fumarate is a competitive inhibitor of 2-oxoglutarate-dependent lysine demethylase (KDM) family of histone lysine demethylases,[51] we determined the effect of PDM on histone lysine methylation marks and observed a major decrease in H3K9me3 and H3K4me1 (Figure S6D). We focused on H3K9me3 since it is associated with heterochromatin-induced gene silencing. Chromatin immunoprecipitation (ChIP) analysis revealed the enrichment of H3K9me3 mark in the −(870–664) region of *ASB11* promoter (Figure S6E), and furthermore, deposition of this mark was greatly decreased by PDM (Figures 6D and S6F). Supplement of PDM-treated cells with monomethyl fumarate (MMF), a cell-permeable derivative of fumarate, rescued H3K9me3 deposition on *ASB11* promoter and abolished PDM-induced upregulation of *ASB11* mRNA and protein to suppress endogenous purinosome formation (Figures 6E–6G and S6G–S6I). Similar effects were observed with arginine supplementation, which rescued cellular fumarate level (Figure S6J), presumably by replenishing urea cycle metabolites. Supplement of PDM-treated cells with inosine to increase intracellular purines also rescued H3K9me3 deposition on *ASB11* promoter (Figure S6K). Thus, PDM reduces fumarate to relieve H3K9me3-mediated epigenetic silencing of *ASB11* (Figure 6H).

Similarly, antimycin A treatment reduced fumarate, H3K9me3 level, and H3K9me3 deposition on *ASB11* promoter (Figures 6I, 6J, and S6L). MMF or arginine supplement reverted the effects of antimycin A on H3K9m3 modification of *ASB11* promoter, *ASB11* mRNA expression, and purinosome formation (Figures 6J–6L). Arginine supplement also reverted fumarate level in antimycin A-treated cells (Figure 6I). Likewise, SHIN1 treatment reduced fumarate and decreased H3K9me3 occupancy on *ASB11* promoter (Figures S6M and S6N). MMF or arginine supplement of SHIN1-treated cells rescued H3K9me3 deposition, thereby reducing *ASB11* expression and blocking SHIN1-induced purinosome and endogenous purinosome

Figure 5. Purinosome formation enhances DNPS pathway flux and is induced by DNPS blockage

(A) Schematic of $^{13}C_6$-glucose labeling into purines.

(B and G) HeLa cells stably expressing IPTG-inducible PAICS shRNA and Dox-inducible PAICS WT or mutant cDNA and treated with 500 μM IPTG and 1 μg/mL Dox for 4 days. Cells were treated with DMAT or antimycin A for 12 h and labeled with $^{13}C_6$-glucose for 5 min. The intracellular levels of tracer were determined and presented as relative peak area. The equal expression of PAICS WT and mutant is shown on the right of (B).

(C–F and H–J) Fractional abundance of indicated ^{13}C-labeled purine intermediates in HeLa cell derivatives treated as in (B) and labeled with $^{13}C_6$-glucose for 14 h.

(K) Schematic of the role of SHIN1in blocking DNPS.

(L) Purinosome formation in HeLa cells treated with SHIN1.

(M and O) Purinosome formation in HeLa cells transfected with mEos2-FGAMS and ASB11 siRNA (M) or HeLa UBAP2 KO cells transfected with mEos2-FGAMS (O), and cells were treated with SHIN1. The expression of ASB11 is shown.

(N) Purinosome formation in PAICS replacement cells treated as in (B), transfected with mEOS2-FGAMS and treated with SHIN1. Quantitative data in all panels are mean ± SD; n = 3, $^{**}p < 0.01$ and $^{***}p < 0.001$ by unpaired t test (B–J, L, M, and O) or one-way ANOVA with Tukey's multiple comparisons test (N); ns, not significant. Scale bars, 10 μm.

(P) PAICS ubiquitination in HeLa cells transfected with indicated constructs and treated with SHIN1. Asterisk denotes a non-specific band.

Please cite this article in press as: Chou et al., PAICS ubiquitination recruits UBAP2 to trigger phase separation for purinosome assembly, Molecular Cell (2023), https://doi.org/10.1016/j.molcel.2023.09.028

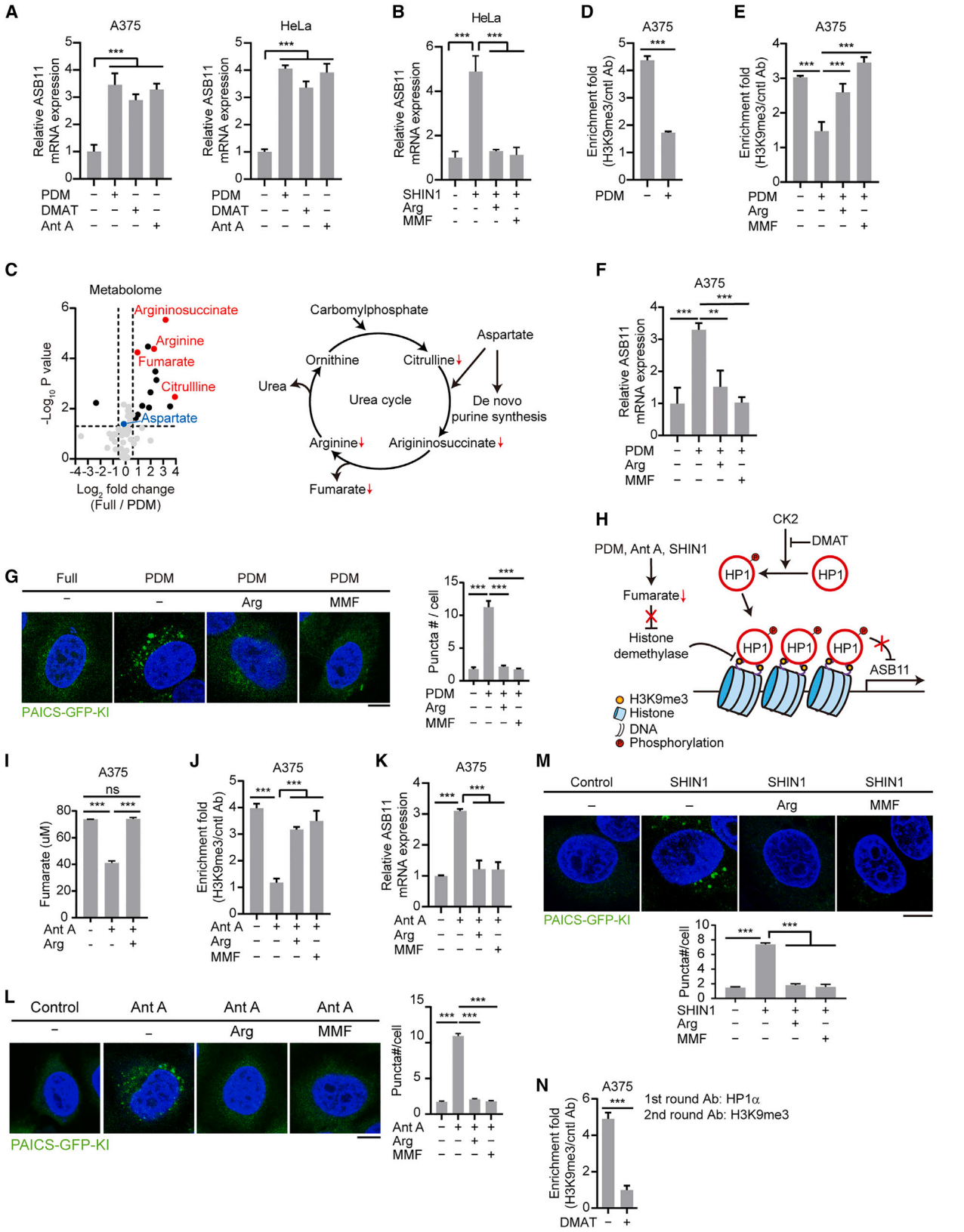

(legend on next page)

Please cite this article in press as: Chou et al., PAICS ubiquitination recruits UBAP2 to trigger phase separation for purinosome assembly, Molecular Cell (2023), https://doi.org/10.1016/j.molcel.2023.09.028

formation (Figures 6B, 6M, S6N, and S6O). Inosine supplement also reverted SHIN1-induced *ASB11* mRNA and protein expression (Figures S6C and S6P). Thus, antimycin A and SHIN1 elevate *ASB11* expression through the same epigenetic mechanism as PDM treatment (Figure 6H).

DMAT, however, did not affect H3K9me3 deposition on *ASB11* promotor (Figure S6Q), indicating the utilization of a different mechanism. The heterochromatin protein 1 (HP1) is a "reader" of H3K9me3 to facilitate heterochromatin formation.[52] Previous studies reported that CK2-mediated phosphorylation of HP1α increases its binding to H3K9me3.[53,54] Accordingly, DMAT greatly diminished the deposition of H3K9me3/HP1α complex on *ASB11* promoter, as demonstrated by Re-ChIP analysis (Figure 6N). Thus, DMAT impairs the recruitment of HP1α to H3K9me3-occupied *ASB11* promoter, which likely contributes to a de-repression of *ASB11* transcription (Figure 6H).

Constitutive purinosome formation in melanoma by ASB11 high expression supports malignant progression

Next, we interrogated the impacts of purinosomes on disease states. Tumor cells often rely on DNPS to meet the metabolic requirement for their proliferation.[15] By querying The Cancer Genome Atlas (TCGA) datasets of 17 cancer types, we found that *ASB11* mRNA is specifically enriched in melanoma (Figure S7A). Furthermore, *ASB11* mRNA levels are higher in the primary and metastatic melanoma, compared with normal skin tissue (Figure 7A). Accordingly, human melanoma cell lines A375 and WM115 expressed higher levels of *ASB11* mRNA than HeLa cells (Figure S7B). PAICS ubiquitination level was also higher in A375 than HeLa cells (Figure S7C). Consequently, A375 and WM115 cells exhibited constitutive purinosome formation in purine-rich medium, and ASB11 depletion significantly reduced purinosomes (Figures 7B, 7C, and S7D). Furthermore, replacement of PAICS WT with K74R mutant or KD of UBAP2 diminished the numbers of constitutive purinosomes formed in A375 cells (Figures S7E and S7F). Consistent with the constitutive purinosome formation, immunoprecipitation detected the interaction between endogenous PAICS and endogenous UBAP2 in A375 cells, which was abrogated by ASB11 silencing (Figure 7D). Thus, the elevated ASB11 expression in melanoma confers a constitutive purinosome formation through a mechanism resembling extracellular purine depletion.

Importantly, ASB11 KD, replacement of PAICS WT with K74R mutant, or UBAP2 KD each compromised proliferation and viability of A375 cells (Figures 7E–7J and S7G–S7I). Reconstitution of UBAP2-depleted A375 cells with UBA2 WT, but not ΔUBA or ΔIDR mutant, rescued cell proliferation and viability (Figures 7I, 7J, S7J, and S7K). Furthermore, the impaired proliferation and viability seen in ASB11 KD cells, PAICS K74R reconstituted cells, UBAP2 KD cells, and UBAP2ΔUBA reconstituted cells were all rescued by supplement of cells with adenosine and guanosine (Figures S7L–S7S), suggesting that insufficient purine availability accounts for the proliferation and viability defects seen in these purinosome-deficient conditions. Moreover, using an orthotopic model, we showed that ASB11 depletion, replacement of PAICS WT with K74R mutant, or UBAP2 depletion each retarded the growth of A375-derived tumors. The impaired tumor growth by UBAP2 KD was rescued by re-expressing UBAP2 WT but not UBAP2ΔUBA (Figures 7K–7M). We conclude that melanoma cells are addicted to constitutive purinosome formation to support their proliferation, viability, and tumorigenesis.

DISCUSSION

This study identifies a Ub-dependent mechanism mediating purinosome assembly (Figure 7N). In response to several purinosome-inducing cues, the expression of ASB11 is elevated through epigenetic mechanisms, thereby inducing non-degradable K6-polyubiquitination on DNPS enzyme PAICS. This ubiquitination facilitates PAICS interaction with UBAP2 to trigger LLPS. Notably, the multivalent interactions mediated by IDRs in UBAP2 and by UBAP2 UBA domain binding to polyUb are both necessary for this LLPS. We provide evidence indicating that the coordinated phase separation of polyubiquitinated PAICS with UBAP2 represents a major driving force for purinosome assembly. Other DNPS enzymes are likely recruited by two non-mutually exclusive mechanisms. First, they are associated with PAICS before the formation of microscopically visible purinosomes,[4] and PAICS polyubiquitination-induced phase separation with UBAP2 coalesces numerous pre-existing DNPS enzyme complexes into a large condensate. Additionally, upon phase separation, the IDRs of UBAP2 might be able to recruit more DNPS enzymes through a direct or indirect mechanism. The enrichment of DNPS enzymes and metabolites in purinosomes eventually enhances the efficiency of DNPS pathway.

The unraveling of purinosome assembly mechanism provides us with an initial opportunity to elucidate the pathophysiological function of purinosomes. We show that purinosomes are constitutively formed in melanoma cells due to ASB11 high expression.

Figure 6. Purinosome-inducing cues elevate ASB11 expression through epigenetic mechanisms

(A, B, F, and K) *ASB11* mRNA levels in cells treated with indicated agents.

(C) Left: volcano plot of metabolite level changes identified from A375 cells cultured in full medium or PDM for 6 h. Right: the connection of urea cycle to DNPS pathway. Metabolites downregulated by PDM are marked.

(D, E, and J) H3K9me3 occupancy on *ASB11* promoter in cells treated with indicated agents for 6 h (D) or 16 h (E and J).

(G, L, and M) Endogenous purinosome formation in HeLa GFP_{11} knockin cells transfected with GFP_{1-10} and treated with indicated agents for 16 h (G and L) or 48 h (M). Scale bars, 10 μm.

(H) A model depicting epigenetic mechanisms underpinning *ASB11* mRNA upregulation by various agents.

(I) Fumarate levels in cells treated with indicated agents.

(N) Re-ChIP assay for H3K9me3/HP1α complex occupancy on *ASB11* promoter in DMAT-treated cells. The enrichment folds are normalized with those with control antibody in the 1st round of ChIP. Quantitative data in all panels are mean ± SD; n = 3, *$p < 0.05$ and ***$p < 0.001$ by one-way ANOVA with Dunnett's multiple comparisons test (A and I), unpaired t test (D and M), or one-way ANOVA with Tukey's multiple comparisons test (B, E–G, J–L, and M). See also Figure S6 and Table S4.

Please cite this article in press as: Chou et al., PAICS ubiquitination recruits UBAP2 to trigger phase separation for purinosome assembly, Molecular Cell (2023), https://doi.org/10.1016/j.molcel.2023.09.028

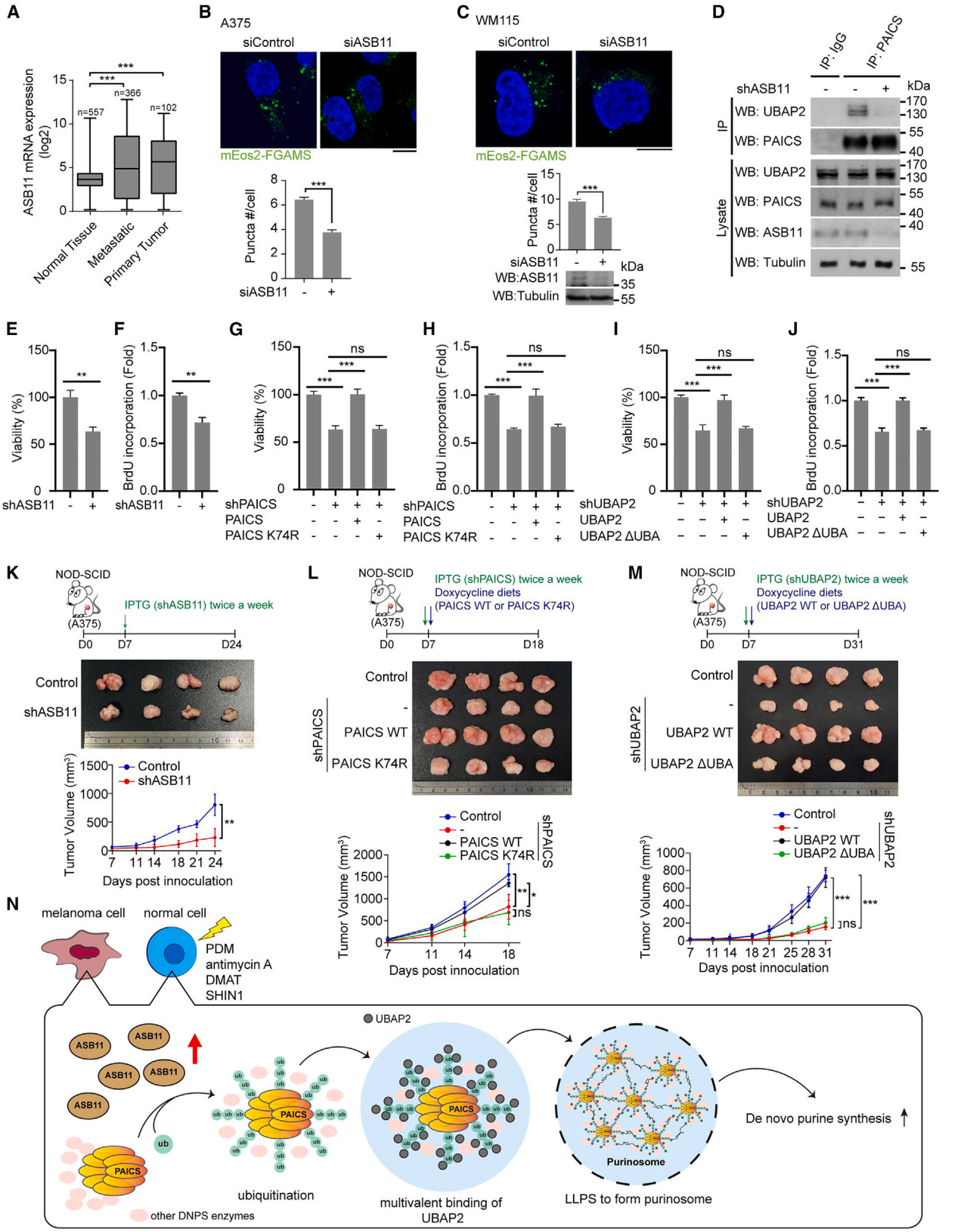

(legend on next page)

Please cite this article in press as: Chou et al., PAICS ubiquitination recruits UBAP2 to trigger phase separation for purinosome assembly, Molecular Cell (2023), https://doi.org/10.1016/j.molcel.2023.09.028

Furthermore, inhibition of purinosome assembly by blocking PAICS ubiquitination or PAICS interaction with UBAP2 impairs melanoma cell proliferation and survival *in vitro* and tumorigenesis *in vivo* (Figure 7N). These tumor-suppressive effects of purinosome disruption are most likely mediated by purine deficiency, as supplement of cells with adenosine and guanosine reverses these effects. Our findings thus support that melanoma cells are addicted to purinosome formation and highlight a protumor function of purinosomes. Notably, the impact of purinosome formation on tumors might not be restricted to melanoma. Hypoxia, an essential and common feature of microenvironment for solid cancers, also induces purinosomes,[55] even though the impact of purinosome formation on hypoxic cells remains elusive and warrants further analysis.

Our study has developed a method allowing for purinosome detection at the endogenous level. A long-lasting concern on the physiological relevance of purinosomes lies in the detection method; that is, overexpression of a fluorescently tagged DNPS enzyme has been commonly used in the field. Although coimmunoprecipitation and PLA were recently included to detect the interactions among DNPS enzymes endogenously,[4,55] they cannot reveal the formation of condensate-like structure. In contrast, the split-GFP KI strategy established in this study not only enables the visualization of purinosomes at the endogenous levels but also confirms many previous findings derived from the DNPS enzyme overexpression system, such as the induction of purinosomes by several stressed conditions and the liquid condensate-like properties of purinosomes. Although our study used the split-GFP system for an efficient KI by introducing the small GFP_{11} fragment, KI of the entire GFP is also technically feasible. In the future, the GFP KI strategy can be applied to generate reporter animals for studying purinosome formation and functions *in vivo*.

Notably, blockage of PAICS ubiquitination-mediated purinosome assembly pathway by ASB11 or UBAP2 depletion or PAICS K74R mutation significantly reduces but not completely eliminates purinosomes. These findings suggest the existence of an additional mechanism that cooperates with the PAICS-ubiquitination-dependent mechanism to form purinosomes. Formation of microscopically visible condensates via multiple independent pathways or even multiple molecular stages has been reported for other condensates such as stress granules.[56] Future studies will aim to identify additional driving mechanisms for purinosome assembly.

We show that PDM decreases several urea cycle metabolites without significantly affecting aspartate level (Figure 6C; Table S4), suggesting an increased input of aspartate to the DNPS pathway for replenishing cellular purine pool, at the expense of urea cycle metabolites. The decreased fumarate contributes to *ASB11* upregulation by reducing the H3K9me3 repressive mark on *ASB11* promoter. Interesting, antimycin A and SHIN1 treatment similarly downregulates fumarate and induces *ASB11* expression through the same epigenetic mechanism. Despite these findings, we cannot exclude the possibility of an involvement of other mechanisms in ASB11 induction by these purinosome-inducing cues. Future studies are needed to further dissect the detailed mechanisms underlying the regulation of cellular fumarate level and ASB11 expression by various purinosome-inducing cues.

In summary, our study identifies a Ub-dependent mechanism that drives purinosome assembly through LLPS and elucidates the impacts of this purinosome assembly mechanism on the malignancies of melanoma.

Limitations of the study

This study identifies the critical role of ASB11-PAICS-UBAP2 axis in the assembly of purinosome. However, ablation of each component in this axis greatly reduces, but not completely eliminates, purinosome formation, indicating the involvement of additional and uncharacterized mechanisms in the purinosome assembly process. In addition, although this study uncovers the fumarate downregulation-induced epigenetic change on *ASB11* gene as a trigger for purinosome assembly, the detailed mechanisms underlying this fumarate level changes in response to several purinosome-inducing cues remain to be determined.

STAR★METHODS

Detailed methods are provided in the online version of this paper and include the following:

- KEY RESOURCES TABLE
- RESOURCE AVAILABILITY
  - Lead contact
  - Materials availability
  - Data and code availability
- EXPERIMENTAL MODEL AND STUDY PARTICIPANT DETAILS
  - *E. coli* strains
  - Mammalian cell culture and transfection
  - Mice
- METHOD DETAILS

Figure 7. Constitutive purinosome formation in melanoma by ASB11 high expression supports malignant progression

(A) *ASB11* mRNA levels presented by whiskers boxplot, ***$p < 0.001$ by one-way ANOVA with Dunnett's multiple comparisons test.

(B and C) Purinosome formation in cells transfected with mEos2-FGAMS and ASB11 siRNA and cultured in full medium. The knockdown efficiencies of ASB11 siRNA in A375 and WM115 cells are shown in Figure 2D (the same experiment) and at the bottom, respectively. Scale bars, 10 μm.

(D) UBAP2-PAICS interaction in A375 cells stably expressing IPTG-inducible ASB11 shRNA and treated with IPTG for 5 days.

(E–J) MTT (E, G, and I) or BrdU (F, H, and J) assay for A375 cells stably expressing IPTG-inducible shRNAs and Dox-inducible rescue cDNAs and treated with IPTG and Dox for 5 days. The knockdown efficiencies of various shRNAs and the expression levels of various rescued proteins are shown in Figures S7G–S7I.

(K–M) Mice inoculated with A375 derivatives as in (D)–(F) were injected with IPTG and/or fed with Dox-containing diets (top). Tumor growth curves (bottom) and tumor sizes at the final day (middle) are shown.

(N) Schematic of the PAICS ubiquitination-mediated purinosome assembly mechanism, its regulation by purinosome-inducing cues, and its impacts on melanoma. Quantitative data are mean ± SD; n = 3 (B, C, and E–J) or n = 4 (K–M); **$p < 0.01$ and ***$p < 0.001$ by unpaired t test (B, C, E, F, and K) or one-way ANOVA with Tukey's multiple comparisons test (G–J, L, and M); ns, not significant. See also Figure S7.

Please cite this article in press as: Chou et al., PAICS ubiquitination recruits UBAP2 to trigger phase separation for purinosome assembly, Molecular Cell (2023), https://doi.org/10.1016/j.molcel.2023.09.028

- Plasmids
- Lentiviral production and infection
- RT-qPCR
- RNA interference
- Immunoprecipitation
- In vivo ubiquitination assay
- In vitro ubiquitination assay
- In vitro deubiquitination by USP30
- Baculovirus protein expression and purification
- Purinosome induction and detection by fluorescence microscopy
- Quantification of puncta number and colocalization
- Time-lapse fluorescence imaging
- PLA
- ChIP and Re-ChIP assays
- Quantitative ubiquitylome and proteome analyses by SILAC labeling and LC-MS/MS
- Proximity biotinylation by TurboID
- Label-free quantitative LC-MS/MS analysis
- Determination of ubiquitination sites by LC-MS/MS
- Metabolite profiling analysis
- Isotope labeling and metabolic flux assay
- Gene editing by CRISPR
- Fumarate assay
- PAICS activity assay
- Far-UV CD spectroscopy
- Protein expression and purification
- Generation of K6-linked polyUb chain
- In vitro phase separation assay
- FRAP assay
- Biolayer interferometry (BLI) analysis
- Cell viability and proliferation assays
- Animal studies

● QUANTIFICATION AND STATISTICAL ANALYSIS

SUPPLEMENTAL INFORMATION

Supplemental information can be found online at https://doi.org/10.1016/j.molcel.2023.09.028.

ACKNOWLEDGMENTS

We thank Yane-Shih Wang, Che-Hung Shen, Ya-Wen Liu, Guang-Chao Chen, and Wei Yuan Yang for reagents; National RNAi Core Facility for shRNA constructs and for generating KO and KI cells; Academia Sinica (AS) Common Mass Spectrometry Facility located at the Institute of Biological Chemistry (IBC) for mass spectrometry analysis; IBC Cell Biology, Biophysics, and Protein Core Facilities for assisting with confocal analysis, CD analysis, and protein purification, respectively; AS Biophysics Core Facility for supporting BLI analysis; Ruei-Liang Yan, Pei-Tzu Chen, and Min-Chi Yeh for technical support; Ping-Chih Ho and Hui-Kuan Lin for discussions; and Chi-Kuang Yao for critically reading the manuscript. This work is supported by NSTC Academic Summit grant no. 111-2639-B-001-001ASP and Academia Sinica Investigator award AS-IA-112-L04.

AUTHOR CONTRIBUTIONS

M.-C.C. and Y.-H.W. designed and performed most experiments and analyzed the data. F.-Y.C. and C.-Y.K. performed some biochemical and cell image analyses, respectively. K.-P.W. supervised protein purification and conducted biophysics analysis. J.-C.K. conducted and supervised FRAP analyses. S.-J.C. helped with animal studies. M.-L.C. and C.-Y.L. conducted metabolomics analysis. Y.-C.C. conducted CRISPR gene editing. M.-C.H. supervised PAICS purification and activity assay. S.F. provided reagents. J.-r.H. provided guidance on LLPS-related studies. R.-H.C. directed and coordinated study, designed the research, and oversaw the project. M.-C.C., Y.-H.W., F.-Y.C., and R.-H.C. wrote the manuscript.

DECLARATION OF INTERESTS

The authors declare no competing interests.

INCLUSION AND DIVERSITY

We support inclusive, diverse, and equitable conduct of research.

Received: January 16, 2023
Revised: July 10, 2023
Accepted: September 22, 2023
Published: October 16, 2023

REFERENCES

1. Srere, P.A. (1985). The metabolon. Trends Biochem. Sci. *10*, 109–110. https://doi.org/10.1016/0968-0004(85)90266-X.
2. Sweetlove, L.J., and Fernie, A.R. (2018). The role of dynamic enzyme assemblies and substrate channelling in metabolic regulation. Nat. Commun. *9*, 2136. https://doi.org/10.1038/s41467-018-04543-8.
3. An, S., Kumar, R., Sheets, E.D., and Benkovic, S.J. (2008). Reversible compartmentalization of de novo purine biosynthetic complexes in living cells. Science *320*, 103–106. https://doi.org/10.1126/science.1152241.
4. He, J., Zou, L.N., Pareek, V., and Benkovic, S.J. (2022). Multienzyme interactions of the de novo purine biosynthetic protein PAICS facilitate purinosome formation and metabolic channeling. J. Biol. Chem. *298*, 101853. https://doi.org/10.1016/j.jbc.2022.101853.
5. Pedley, A.M., Pareek, V., and Benkovic, S.J. (2022). The purinosome: A case study for a mammalian metabolon. Annu. Rev. Biochem. *91*, 89–106. https://doi.org/10.1146/annurev-biochem-032620-105728.
6. Zhao, H., Chiaro, C.R., Zhang, L., Smith, P.B., Chan, C.Y., Pedley, A.M., Pugh, R.J., French, J.B., Patterson, A.D., and Benkovic, S.J. (2015). Quantitative analysis of purine nucleotides indicates that purinosomes increase de novo purine biosynthesis. J. Biol. Chem. *290*, 6705–6713. https://doi.org/10.1074/jbc.M114.628701.
7. An, S., Kyoung, M., Allen, J.J., Shokat, K.M., and Benkovic, S.J. (2010). Dynamic regulation of a metabolic multi-enzyme complex by protein kinase CK2. J. Biol. Chem. *285*, 11093–11099. https://doi.org/10.1074/jbc.M110.101139.
8. French, J.B., Jones, S.A., Deng, H., Pedley, A.M., Kim, D., Chan, C.Y., Hu, H., Pugh, R.J., Zhao, H., Zhang, Y., et al. (2016). Spatial colocalization and functional link of purinosomes with mitochondria. Science *351*, 733–737. https://doi.org/10.1126/science.aac6054.
9. Pedley, A.M., and Benkovic, S.J. (2017). A new view into the regulation of purine metabolism: the purinosome. Trends Biochem. Sci. *42*, 141–154. https://doi.org/10.1016/j.tibs.2016.09.009.
10. Verrier, F., An, S., Ferrie, A.M., Sun, H., Kyoung, M., Deng, H., Fang, Y., and Benkovic, S.J. (2011). GPCRs regulate the assembly of a multienzyme complex for purine biosynthesis. Nat. Chem. Biol. *7*, 909–915. https://doi.org/10.1038/nchembio.690.
11. Pareek, V., Tian, H., Winograd, N., and Benkovic, S.J. (2020). Metabolomics and mass spectrometry imaging reveal channeled de novo purine synthesis in cells. Science *368*, 283–290. https://doi.org/10.1126/science.aaz6465.
12. Kyoung, M., Russell, S.J., Kohnhorst, C.L., Esemoto, N.N., and An, S. (2015). Dynamic architecture of the purinosome involved in human de novo purine biosynthesis. Biochemistry *54*, 870–880. https://doi.org/10.1021/bi501480d.

Please cite this article in press as: Chou et al., PAICS ubiquitination recruits UBAP2 to trigger phase separation for purinosome assembly, Molecular Cell (2023), https://doi.org/10.1016/j.molcel.2023.09.028

13. Pedley, A.M., Boylan, J.P., Chan, C.Y., Kennedy, E.L., Kyoung, M., and Benkovic, S.J. (2022). Purine biosynthetic enzymes assemble into liquid-like condensates dependent on the activity of chaperone protein HSP90. J. Biol. Chem. *298*, 101845. https://doi.org/10.1016/j.jbc.2022.101845.

14. Markmiller, S., Soltanieh, S., Server, K.L., Mak, R., Jin, W., Fang, M.Y., Luo, E.C., Krach, F., Yang, D., Sen, A., et al. (2018). Context-dependent and disease-specific diversity in protein interactions within stress granules. Cell *172*, 590–604.e13. https://doi.org/10.1016/j.cell.2017.12.032.

15. Villa, E., Ali, E.S., Sahu, U., and Ben-Sahra, I. (2019). Cancer cells tune the signaling pathways to empower de novo synthesis of nucleotides. Cancers (Basel) *11*, 688. https://doi.org/10.3390/cancers11050688.

16. De Vitto, H., Arachchige, D.B., Richardson, B.C., and French, J.B. (2021). The intersection of purine and mitochondrial metabolism in cancer. Cells *10*, 2603. https://doi.org/10.3390/cells10102603.

17. Ali, E.S., Sahu, U., Villa, E., O'Hara, B.P., Gao, P., Beaudet, C., Wood, A.W., Asara, J.M., and Ben-Sahra, I. (2020). ERK2 phosphorylates PFAS to mediate posttranslational control of de novo purine synthesis. Mol. Cell *78*, 1178–1191.e6. https://doi.org/10.1016/j.molcel.2020.05.001.

18. Lv, Y., Wang, X., Li, X., Xu, G., Bai, Y., Wu, J., Piao, Y., Shi, Y., Xiang, R., and Wang, L. (2020). Nucleotide de novo synthesis increases breast cancer stemness and metastasis via cGMP-PKG-MAPK signaling pathway. PLOS Biol. *18*, e3000872. https://doi.org/10.1371/journal.pbio.3000872.

19. Wang, X., Yang, K., Xie, Q., Wu, Q., Mack, S.C., Shi, Y., Kim, L.J.Y., Prager, B.C., Flavahan, W.A., Liu, X., et al. (2017). Purine synthesis promotes maintenance of brain tumor initiating cells in glioma. Nat. Neurosci. *20*, 661–673. https://doi.org/10.1038/nn.4537.

20. Zhou, W., Yao, Y., Scott, A.J., Wilder-Romans, K., Dresser, J.J., Werner, C.K., Sun, H., Pratt, D., Sajjakulnukit, P., Zhao, S.G., et al. (2020). Purine metabolism regulates DNA repair and therapy resistance in glioblastoma. Nat. Commun. *11*, 3811. https://doi.org/10.1038/s41467-020-17512-x.

21. Alberti, S., and Hyman, A.A. (2021). Biomolecular condensates at the nexus of cellular stress, protein aggregation disease and ageing. Nat. Rev. Mol. Cell Biol. *22*, 196–213. https://doi.org/10.1038/s41580-020-00326-6.

22. Banani, S.F., Lee, H.O., Hyman, A.A., and Rosen, M.K. (2017). Biomolecular condensates: organizers of cellular biochemistry. Nat. Rev. Mol. Cell Biol. *18*, 285–298. https://doi.org/10.1038/nrm.2017.7.

23. Shin, Y., and Brangwynne, C.P. (2017). Liquid phase condensation in cell physiology and disease. Science *357*, eaaf4382. https://doi.org/10.1126/science.aaf4382.

24. Choi, J.M., Holehouse, A.S., and Pappu, R.V. (2020). Physical principles underlying the complex biology of intracellular phase transitions. Annu. Rev. Biophys. *49*, 107–133. https://doi.org/10.1146/annurev-biophys-121219-081629.

25. Nott, T.J., Petsalaki, E., Farber, P., Jervis, D., Fussner, E., Plochowietz, A., Craggs, T.D., Bazett-Jones, D.P., Pawson, T., Forman-Kay, J.D., et al. (2015). Phase transition of a disordered nuage protein generates environmentally responsive membraneless organelles. Mol. Cell *57*, 936–947. https://doi.org/10.1016/j.molcel.2015.01.013.

26. Wang, J., Choi, J.M., Holehouse, A.S., Lee, H.O., Zhang, X., Jahnel, M., Maharana, S., Lemaitre, R., Pozniakovsky, A., Drechsel, D., et al. (2018). A molecular grammar governing the driving forces for phase separation of prion-like RNA binding proteins. Cell *174*, 688–699.e16. https://doi.org/10.1016/j.cell.2018.06.006.

27. Jiang, S., Fagman, J.B., Chen, C., Alberti, S., and Liu, B. (2020). Protein phase separation and its role in tumorigenesis. eLife *9*, e60264. https://doi.org/10.7554/eLife.60264.

28. Luo, Y.Y., Wu, J.J., and Li, Y.M. (2021). Regulation of liquid-liquid phase separation with focus on post-translational modifications. Chem. Commun. (Camb) *57*, 13275–13287. https://doi.org/10.1039/d1cc05266g.

29. Dao, T.P., Kolaitis, R.M., Kim, H.J., O'Donovan, K., Martyniak, B., Colicino, E., Hehnly, H., Taylor, J.P., and Castañeda, C.A. (2018). Ubiquitin modulates liquid-liquid phase separation of UBQLN2 via disruption of multivalent interactions. Mol. Cell *69*, 965–978.e6. https://doi.org/10.1016/j.molcel.2018.02.004.

30. Gwon, Y., Maxwell, B.A., Kolaitis, R.M., Zhang, P., Kim, H.J., and Taylor, J.P. (2021). Ubiquitination of G3BP1 mediates stress granule disassembly in a context-specific manner. Science *372*, eabf6548. https://doi.org/10.1126/science.abf6548.

31. Peng, S.Z., Chen, X.H., Chen, S.J., Zhang, J., Wang, C.Y., Liu, W.R., Zhang, D., Su, Y., and Zhang, X.K. (2021). Phase separation of Nur77 mediates celastrol-induced mitophagy by promoting the liquidity of p62/SQSTM1 condensates. Nat. Commun. *12*, 5989. https://doi.org/10.1038/s41467-021-26295-8.

32. Sun, D., Wu, R., Zheng, J., Li, P., and Yu, L. (2018). Polyubiquitin chain-induced p62 phase separation drives autophagic cargo segregation. Cell Res. *28*, 405–415. https://doi.org/10.1038/s41422-018-0017-7.

33. Zaffagnini, G., Savova, A., Danieli, A., Romanov, J., Tremel, S., Ebner, M., Peterbauer, T., Sztacho, M., Trapannone, R., Tarafder, A.K., et al. (2018). p62 filaments capture and present ubiquitinated cargos for autophagy. EMBO J. *37*, e98308. https://doi.org/10.15252/embj.201798308.

34. Yasuda, S., Tsuchiya, H., Kaiho, A., Guo, Q., Ikeuchi, K., Endo, A., Arai, N., Ohtake, F., Murata, S., Inada, T., et al. (2020). Stress- and ubiquitylation-dependent phase separation of the proteasome. Nature *578*, 296–300. https://doi.org/10.1038/s41586-020-1982-9.

35. Du, M., Ea, C.K., Fang, Y., and Chen, Z.J. (2022). Liquid phase separation of NEMO induced by polyubiquitin chains activates NF-kappaB. Mol. Cell *82*, 2415–2426.e5. https://doi.org/10.1016/j.molcel.2022.03.037.

36. Goel, S., Oliva, R., Jeganathan, S., Bader, V., Krause, L.J., Kriegler, S., Stender, I.D., Christine, C.W., Nakamura, K., Hoffmann, J.E., et al. (2023). Linear ubiquitination induces NEMO phase separation to activate NF-kappaB signaling. Life Sci. Alliance *6*, e202201607. https://doi.org/10.26508/lsa.202201607.

37. Banjade, S., Zhu, L., Jorgensen, J.R., Suzuki, S.W., and Emr, S.D. (2022). Recruitment and organization of ESCRT-0 and ubiquitinated cargo via condensation. Sci. Adv. *8*, eabm5149. https://doi.org/10.1126/sciadv.abm5149.

38. Dao, T.P., Yang, Y., Presti, M.F., Cosgrove, M.S., Hopkins, J.B., Ma, W., Loh, S.N., and Castañeda, C.A. (2022). Mechanistic insights into enhancement or inhibition of phase separation by different polyubiquitin chains. EMBO Rep. *23*, e55056. https://doi.org/10.15252/embr.202255056.

39. Vamadevan, V., Chaudhary, N., and Maddika, S. (2022). Ubiquitin-assisted phase separation of dishevelled-2 promotes Wnt signalling. J. Cell Sci. *135*, jcs260284. https://doi.org/10.1242/jcs.260284.

40. Andresen, C.A., Smedegaard, S., Sylvestersen, K.B., Svensson, C., Iglesias-Gato, D., Cazzamali, G., Nielsen, T.K., Nielsen, M.L., and Flores-Morales, A. (2014). Protein interaction screening for the ankyrin repeats and suppressor of cytokine signaling (SOCS) box (ASB) family identify Asb11 as a novel endoplasmic reticulum resident ubiquitin ligase. J. Biol. Chem. *289*, 2043–2054. https://doi.org/10.1074/jbc.M113.534602.

41. Chen, F.Y., Huang, M.Y., Lin, Y.M., Ho, C.H., Lin, S.Y., Chen, H.Y., Hung, M.C., and Chen, R.H. (2019). BIK ubiquitination by the E3 ligase Cul5-ASB11 determines cell fate during cellular stress. J. Cell Biol. *218*, 3002–3018. https://doi.org/10.1083/jcb.201901156.

42. Theurillat, J.P., Udeshi, N.D., Errington, W.J., Svinkina, T., Baca, S.C., Pop, M., Wild, P.J., Blattner, M., Groner, A.C., Rubin, M.A., et al. (2014). Prostate cancer. Ubiquitylome analysis identifies dysregulation of effector substrates in SPOP-mutant prostate cancer. Science *346*, 85–89. https://doi.org/10.1126/science.1250255.

43. Cunningham, C.N., Baughman, J.M., Phu, L., Tea, J.S., Yu, C., Coons, M., Kirkpatrick, D.S., Bingol, B., and Corn, J.E. (2015). USP30 and parkin homeostatically regulate atypical ubiquitin chains on mitochondria. Nat. Cell Biol. *17*, 160–169. https://doi.org/10.1038/ncb3097.

Please cite this article in press as: Chou et al., PAICS ubiquitination recruits UBAP2 to trigger phase separation for purinosome assembly, Molecular Cell (2023), https://doi.org/10.1016/j.molcel.2023.09.028

44. Swatek, K.N., Usher, J.L., Kueck, A.F., Gladkova, C., Mevissen, T.E.T., Pruneda, J.N., Skern, T., and Komander, D. (2019). Insights into ubiquitin chain architecture using Ub-clipping. Nature *572*, 533–537. https://doi.org/10.1038/s41586-019-1482-y.

45. Leonetti, M.D., Sekine, S., Kamiyama, D., Weissman, J.S., and Huang, B. (2016). A scalable strategy for high-throughput GFP tagging of endogenous human proteins. Proc. Natl. Acad. Sci. USA *113*, E3501–E3508. https://doi.org/10.1073/pnas.1606731113.

46. Li, S.X., Tong, Y.P., Xie, X.C., Wang, Q.H., Zhou, H.N., Han, Y., Zhang, Z.Y., Gao, W., Li, S.G., Zhang, X.C., et al. (2007). Octameric structure of the human bifunctional enzyme PAICS in purine biosynthesis. J. Mol. Biol. *366*, 1603–1614. https://doi.org/10.1016/j.jmb.2006.12.027.

47. Zhou, J., Xu, Y., Lin, S., Guo, Y., Deng, W., Zhang, Y., Guo, A., and Xue, Y. (2018). iUUCD 2.0: an update with rich annotations for ubiquitin and ubiquitin-like conjugations. Nucleic Acids Res. *46*, D447–D453. https://doi.org/10.1093/nar/gkx1041.

48. Hospenthal, M.K., Freund, S.M., and Komander, D. (2013). Assembly, analysis and architecture of atypical ubiquitin chains. Nat. Struct. Mol. Biol. *20*, 555–565. https://doi.org/10.1038/nsmb.2547.

49. Cappello, A., Mancini, M., Madonna, S., Rinaldo, S., Paone, A., Scarponi, C., Belardo, A., Zolla, L., Zuccotti, A., Panatta, E., et al. (2022). Extracellular serine empowers epidermal proliferation and psoriasis-like symptoms. Sci. Adv. *8*, eabm7902. https://doi.org/10.1126/sciadv.abm7902.

50. Thakur, C., and Chen, F. (2019). Connections between metabolism and epigenetics in cancers. Semin. Cancer Biol. *57*, 52–58. https://doi.org/10.1016/j.semcancer.2019.06.006.

51. Losman, J.A., Koivunen, P., and Kaelin, W.G., Jr. (2020). 2-oxoglutarate-dependent dioxygenases in cancer. Nat. Rev. Cancer *20*, 710–726. https://doi.org/10.1038/s41568-020-00303-3.

52. Canzio, D., Chang, E.Y., Shankar, S., Kuchenbecker, K.M., Simon, M.D., Madhani, H.D., Narlikar, G.J., and Al-Sady, B. (2011). Chromodomain-mediated oligomerization of HP1 suggests a nucleosome-bridging mechanism for heterochromatin assembly. Mol. Cell *41*, 67–81. https://doi.org/10.1016/j.molcel.2010.12.016.

53. Hiragami-Hamada, K., Shinmyozu, K., Hamada, D., Tatsu, Y., Uegaki, K., Fujiwara, S., and Nakayama, J. (2011). N-terminal phosphorylation of HP1 {alpha} promotes its chromatin binding. Mol. Cell. Biol. *31*, 1186–1200. https://doi.org/10.1128/MCB.01012-10.

54. Nishibuchi, G., Machida, S., Osakabe, A., Murakoshi, H., Hiragami-Hamada, K., Nakagawa, R., Fischle, W., Nishimura, Y., Kurumizaka, H., Tagami, H., et al. (2014). N-terminal phosphorylation of HP1alpha increases its nucleosome-binding specificity. Nucleic Acids Res. *42*, 12498–12511. https://doi.org/10.1093/nar/gku995.

55. Doigneaux, C., Pedley, A.M., Mistry, I.N., Papayova, M., Benkovic, S.J., and Tavassoli, A. (2020). Hypoxia drives the assembly of the multienzyme purinosome complex. J. Biol. Chem. *295*, 9551–9566. https://doi.org/10.1074/jbc.RA119.012175.

56. Glauninger, H., Wong Hickernell, C.J., Bard, J.A.M., and Drummond, D.A. (2022). Stressful steps: progress and challenges in understanding stress-induced mRNA condensation and accumulation in stress granules. Mol. Cell *82*, 2544–2556. https://doi.org/10.1016/j.molcel.2022.05.014.

57. Chen, Y.H., Huang, T.Y., Lin, Y.T., Lin, S.Y., Li, W.H., Hsiao, H.J., Yan, R.L., Tang, H.W., Shen, Z.Q., Chen, G.C., et al. (2021). VPS34 K29/K48 branched ubiquitination governed by UBE3C and TRABID regulates autophagy, proteostasis and liver metabolism. Nat. Commun. *12*, 1322. https://doi.org/10.1038/s41467-021-21715-1.

58. Yuan, W.C., Lee, Y.R., Lin, S.Y., Chang, L.Y., Tan, Y.P., Hung, C.C., Kuo, J.C., Liu, C.H., Lin, M.Y., Xu, M., et al. (2014). K33-linked polyubiquitination of coronin 7 by Cul3-KLHL20 ubiquitin E3 ligase regulates protein trafficking. Mol. Cell *54*, 586–600. https://doi.org/10.1016/j.molcel.2014.03.035.

59. Chen, H.Y., Chan, S.J., Liu, X., Wei, A.C., Jian, R.I., Huang, K.W., Lang, Y.D., Shih, J.H., Liao, C.C., Luan, C.L., et al. (2022). Long noncoding RNA Smyca coactivates TGF-beta/Smad and Myc pathways to drive tumor progression. J. Hematol. Oncol. *15*, 85. https://doi.org/10.1186/s13045-022-01306-3.

60. Chiang, S.Y., Wu, H.C., Lin, S.Y., Chen, H.Y., Wang, C.F., Yeh, N.H., Shih, J.H., Huang, Y.S., Kuo, H.C., Chou, S.J., et al. (2021). Usp11 controls cortical neurogenesis and neuronal migration through Sox11 stabilization. Sci. Adv. *7*, eabc6093. https://doi.org/10.1126/sciadv.abc6093.

61. Hsu, S.C., Chen, C.L., Cheng, M.L., Chu, C.Y., Changou, C.A., Yu, Y.L., Yeh, S.D., Kuo, T.C., Kuo, C.C., Chuu, C.P., et al. (2021). Arginine starvation elicits chromatin leakage and cGAS-STING activation via epigenetic silencing of metabolic and DNA-repair genes. Theranostics *11*, 7527–7545. https://doi.org/10.7150/thno.54695.

62. Chou, H.Y., Lin, Y.H., Shiu, G.L., Tang, H.Y., Cheng, M.L., Shiao, M.S., and Pai, L.M. (2014). ADI1, a methionine salvage pathway enzyme, is required for Drosophila fecundity. J. Biomed. Sci. *21*, 64. https://doi.org/10.1186/s12929-014-0064-4.

63. Škerlová, J., Unterlass, J., Göttmann, M., Marttila, P., Homan, E., Helleday, T., Jemth, A.S., and Stenmark, P. (2020). Crystal structures of human PAICS reveal substrate and product binding of an emerging cancer target. J. Biol. Chem. *295*, 11656–11668. https://doi.org/10.1074/jbc.RA120.013695.

64. Chiu, Y.P., Sun, Y.C., Qiu, D.C., Lin, Y.H., Chen, Y.Q., Kuo, J.C., and Huang, J.R. (2020). Liquid-liquid phase separation and extracellular multivalent interactions in the tale of galectin-3. Nat. Commun. *11*, 1229. https://doi.org/10.1038/s41467-020-15007-3.

Please cite this article in press as: Chou et al., PAICS ubiquitination recruits UBAP2 to trigger phase separation for purinosome assembly, Molecular Cell (2023), https://doi.org/10.1016/j.molcel.2023.09.028

STAR★METHODS

KEY RESOURCES TABLE

REAGENT or RESOURCE	SOURCE	IDENTIFIER
Antibodies		
6xHis	Takara Bio	Cat# 631212, RRID: AB_2721905
Flag	GeneTex, Sigma-Aldrich	Cat# GTX115043, RRID: AB_11166662 ; Cat# F1804, RRID: AB_262044
Myc	GeneTex, Cell Signaling Technology	Cat# GTX29106, RRID: AB_369669 ; Cat# 2272, RRID: AB_10692100
GST	ABclonal	Cat# AE006, RRID: AB_2771923
HA	Sigma-Aldrich	Cat# H9658, RRID: AB_260092
V5	Millipore	Cat# AB3792, RRID: AB_91591
T7	Millipore	Cat# 69522, RRID: AB_11211744
PAICS	GeneTex	Cat# GTX83950, RRID: AB_10728418 ; Cat# GTX118340, RRID: AB_11172035
ASB11	Customized generation by LTK BioLaboratories Inc.	N/A
FGAMS	Novus Abcam	Cat# NBP1-84691, RRID: AB_11018348 ; Cat# ab251740
ADSL	Novus	Cat# NBP2-03107
GART	Abcam	Cat# ab169550
PPAT	GeneTex	Cat# GTX102725, RRID:AB_11178730
ATIC	GeneTex	Cat# GTX103036, RRID:AB_1949698
K48-linkage Specific Polyubiquitin	Cell Signaling Technology	Cat# 8081, RRID: AB_10859893
K63-linkage Specific Polyubiquitin	Cell Signaling Technology	Cat# 5621, RRID: AB_10827985
Tubulin	GeneTex	Cat# GTX628802, RRID: AB_2716636 ; Cat# GTX112141, RRID: AB_10722892
GAPDH	GeneTex	Cat# GTX100118, RRID: AB_1080976
H3	Cell Signaling Technology	Cat# 9715, RRID: AB_331563
H3K4me1	Abcam	Cat# ab8895, RRID: AB_306847
H3K4me2	Active Motif	Cat# 39679, RRID: AB_2793302
H3K4me3	Abcam	Cat# ab1012, RRID: AB_442796
H3K9me1	Active Motif	Cat# 39887, RRID: AB_2793381
H3K9me2	Active Motif	Cat# 39683, RRID: AB_2793304
H3K9me3	Abcam	Cat# ab176916, RRID: AB_2797591
H3K27me1	Active Motif	Cat# 61015, RRID: AB_2715573
H3K27me2	Active Motif	Cat# 39919, RRID: AB_2793393
H3K27me3	Abcam	Cat# ab192985, RRID: AB_2650559
H3K36me1	Active Motif	Cat# 61351, RRID: AB_2793602
H3K36me2	Active Motif	Cat# 39255, RRID: AB_2793207
H3K36me3	Active Motif	Cat# 61101, RRID: AB_2615073
Mouse IgG	GeneTex	Cat# GTX35009, RRID: AB_10618187
Mouse IgG (HRP)	GE Healthcare	Cat# NA931, RRID: AB_772210
EasyBlot mouse IgG (HRP)	GeneTex	Cat# GTX221667-01, RRID: AB_10728926
Rabbit IgG	Abcam	Cat# ab171870, RRID: AB_2687657
Rabbit IgG (HRP)	GE Healthcare	Cat# NA934, RRID: AB_772206
EasyBlot rabbit IgG (HRP)	GeneTex	Cat# GTX221666-01, RRID: AB_10620421
UBAP2	Abcam	Cat# Ab197083
HP1α	Abclonal	Cat# A3741, RRID:AB_2863134

(*Continued on next page*)

Please cite this article in press as: Chou et al., PAICS ubiquitination recruits UBAP2 to trigger phase separation for purinosome assembly, Molecular Cell (2023), https://doi.org/10.1016/j.molcel.2023.09.028

Continued

REAGENT or RESOURCE	SOURCE	IDENTIFIER
Chemicals, peptides, and recombinant proteins		
Puromycin	Sigma-Aldrich	Cat# P8833, CAS: 58-58-2
Blasticidin	Gibco	Cat# A1113903, CAS: 3513-03-9
Antimycin A	Sigma-Aldrich	Cat# A8674, CAS: 1397-94-0
DMAT	Sigma-Aldrich	Cat# SML2044, CAS: 749234-11-5
Cycloheximide	Sigma-Aldrich	Cat# C7698, CAS: 66-81-9
Doxycycline hyclate	Sigma-Aldrich	Cat# D9891, CAS: 24390-14-5
SHIN1	MCE	Cat# HY-112066, CAS: 2146095-85-2
TRIZOL reagent	Invitrogen	Cat# 15596018, CAS: 9048-46-8
Fluorescein-5-maleimide	Kelowna International Scientific Inc	Cat# AS-81405, CAS: 75350-46-8
L-Arginine monohydrochloride	Sigma-Aldrich	Cat# A6969, CAS: 1119-34-2
mono-Methyl fumarate	Sigma-Aldrich	Cat# 651419, CAS: 2756-87-8
Adenosine	Sigma-Aldrich	Cat# A4036, CAS: 58-61-7
Guanosine	Sigma-Aldrich	Cat# G6264, CAS: 118-00-3
Inosine	Sigma-Aldrich	Cat# I4125, CAS: 58-63-9
FastStart Universal SYBR Green Master reagent	Roche	Cat# 04887352001
MG132	Sigma-Aldrich	Cat# M8699, CAS: 1211877-36-9
methylthiazolyl diphenyl tetrazolium bromide (MTT)	Sigma-Aldrich	Cat# M2128, CAS: 298-93-1
protease inhibitor	Roche	Cat# 04693132001
FLAG Peptide	Sigma-Aldrich	Cat# F3290
Lb^{Pro*}	Chen et al.[57]	N/A
His-Cys-Ub K48R	This paper	N/A
His-UBAP2Δ130-621	This paper	N/A
His-UBAP2ΔIDR	This paper	N/A
His-UBAP2Δ130-621/ΔUBA	This paper	N/A
His-MBP-UBAP2 UBA	This paper	N/A
GST-NleL	This paper	N/A
His-PAICS	This paper	N/A
His-PAICS K74R	This paper	N/A
UBE1	R&D System	Cat# E-305-025
UbcH5a	R&D System	Cat# E2-616
UbcH7	ProSpecbio	Cat# ENZ-342
M1 Tetra-Ubiquitin	South Bay Bio	Cat# SBB-UP0119
K6 Tetra-Ubiquitin	R&D System	Cat# UC-15-025
K11 Tetra-Ubiquitin	R&D System	Cat# UC-45-025
K48 Tetra-Ubiquitin	LifeSensors	Cat# SI-4804-0025
K63 Tetra-Ubiquitin	South Bay Bio	Cat# SBB-UP0073
USP30	Gift from Yane-Shih Wang (Academia Sinica, Taipei, Taiwan)	N/A
Critical commercial assays		
iScript™ cDNA Synthesis Kit	Bio-Rad	Cat# 1708891
Duolink® Proximity Ligation Assay Kit	Sigma-Aldrich	Cat# DUO92004
QIAamp DNA Mini Kit	QIAGEN	Cat# 51306
Pierce High pH Reversed-Phase Peptide Fractionation Kit	Thermo	Cat# 84868
PTMScan ubiquitin remnant motif (K-ε-GG) Kit	Cell Signaling Technology	Cat# 5562

(*Continued on next page*)

Please cite this article in press as: Chou et al., PAICS ubiquitination recruits UBAP2 to trigger phase separation for purinosome assembly, Molecular Cell (2023), https://doi.org/10.1016/j.molcel.2023.09.028

Continued

REAGENT or RESOURCE	SOURCE	IDENTIFIER
Fumarate assay kit	Sigma-Aldrich	Cat# MAK060
ADP-Glo Kinase Assay Kit	Promega	Cat# V9101
Alexa Flour 647 Protein Labeling Kit	Invitrogen	Cat# A20173
BrdU Proliferation Assay Kit	Millipore	Cat# QIA58
Deposited data		
Original MS data (proteins)	This paper	PXD025298 ; PXD038411 ; PXD027946
Western blots and microscopy	This paper	Mendeley Dataset: https://doi.org/10.17632/phgv7p6j5k.4
Original metabolomics data	This paper	MetaboLights: MTBLS8573
Experimental models: Cell lines		
293T	ATCC	CRL-3216
293FT	National RNAi Core Facility, Taipei, Taiwan	N/A
HeLa	ATCC	CCL-2
C2C12	Gift from Ya-Wen Liu (National Taiwan University, Taipei, Taiwan)	N/A
A375	Gift from Che-Hung Shen (National Health Research Institutes, Tainan, Taiwan)	N/A
A2058	Gift from Che-Hung Shen (National Health Research Institutes, Tainan, Taiwan)	N/A
WM115	Gift from Che-Hung Shen (National Health Research Institutes, Tainan, Taiwan)	N/A
Experimental models: Organisms/strains		
Mice: NOD/SCID (NOD.CB17-*Prkdc*^{scid}/NcrCrlBltw)	BioLASCO Co.	N/A
Oligonucleotides		
ON-TARGETplus Human ASB11 siRNA - SMARTpool, see Table S5	Horizon Discovery	Cat# L-013267-00-0020
Primers for qPCR, see Table S5	This paper	N/A
Primers for ChIP-qPCR, see Table S5	This paper	N/A
shRNAs, see Table S5	This paper	N/A
Recombinant DNA		
Myc-ASB11	Chen et al.[41]	N/A
Myc-ASB11ΔSOCS	Chen et al.[41]	N/A
HA-Elongin B	Chen et al.[41]	N/A
T7-Elongin C	Chen et al.[41]	N/A
V5-ROC2	Chen et al.[41]	N/A
Myc-Cul5	Chen et al.[41]	N/A
ASB11-mcherry	This paper	N/A
His-Ub KR mutants	Yuan et al.[58]	N/A
His-Ub K-only mutants	Yuan et al.[58]	N/A
RFP-Ub	Gift from Wei Yuan Yang (Academia Sinica, Taipei, Taiwan)	N/A
3xHA-TurboID-NLS_pCDNA3	Addgene	Cat# 107171
pPAICS-EGFP	Addgene	Cat # 99108
pADSL-EGFP	Addgene	Cat # 99109
pFGAMS-mEos2	Addgene	Cat # 105128
PAICS K/R mutants	This paper	N/A
pRK5-Flag-PAICS	This paper	N/A
pRK5-Flag-PAICS K74R	This paper	N/A

(*Continued on next page*)

Please cite this article in press as: Chou et al., PAICS ubiquitination recruits UBAP2 to trigger phase separation for purinosome assembly, Molecular Cell (2023), https://doi.org/10.1016/j.molcel.2023.09.028

Continued

REAGENT or RESOURCE	SOURCE	IDENTIFIER
pAS4.1w.Pbsd-aOn- PAICS	This paper	N/A
pAS4.1w.Pbsd-aOn- PAICS K74R	This paper	N/A
PAICS-mcherry	This paper	N/A
3xHA-TurboID-ASB11ΔSOCS	This paper	N/A
3xHA-TurboID-PAICS	This paper	N/A
3xHA-TurboID-PAICS K74R	This paper	N/A
UBAP2	ORIGENE	Cat# RG211506
pRK5-Myc-UBAP2	This paper	N/A
UBAP2-mcherry	This paper	N/A
pRK5-Myc-UBAP2ΔUBA	This paper	N/A
pRK5-Myc-UBAP2ΔIDR	This paper	N/A
pRK5-Myc-UBAP2Δ130-202	This paper	N/A
pRK5-Myc-UBAP2Δ130-621	This paper	N/A
pRK5-Myc-UBAP2Δ622-736	This paper	N/A
pRK5-Myc-UBAP2Δ853-966	This paper	N/A
pRK5-Myc-UBAP2Δ982-1119	This paper	N/A
pRK5-Myc-UBAP2 UBA^R	This paper	N/A
pAS4.1w.Pbsd-aOn-UBAP2	This paper	N/A
pAS4.1w.Pbsd-aOn-UBAP2 ΔUBA	This paper	N/A
pVL1392-Myc-UBAP2	This paper	N/A
pVL1392-Myc-UBAP2 ΔUBA	This paper	N/A
pMCSG17-NleL	Addgene	Cat# 66716
pRSFDuet-1-cys-Ub K48R	This paper	N/A
pRSFDuet-1-MBP-UBAP2 UBA	This paper	N/A
pET-28b- PAICS	This paper	N/A
pET-28b- PAICS K74R	This paper	N/A
pPET-28a-UBAP2 Δ130-621	This paper	N/A
pPET-28a-UBAP2 ΔUBA	This paper	N/A
pPET-28a-UBAP2 ΔUBA, Δ130-621	This paper	N/A
pPET-28a-UBAP2 ΔIDR	This paper	N/A
pCMVΔ8.91	National RNAi Core Facility, Taipei, Taiwan	N/A
pMD.G	National RNAi Core Facility, Taipei, Taiwan	N/A
GFP1-10	Addgene	Cat # 80409
Software and algorithms		
ImageJ	National Institutes of Health, Bethesda, MD	https://imagej.nih.gov/ij/
OLYMPUS FV3000 FV31S-SW (v 2.40) software	OLYMPUS	https://www.olympus-lifescience.com/en/downloads/detail-iframe/?0[downloads][id]=847252002
MaxQuant search engine (v1.6.17.0)	Max-Planck-Institute of Biochemistry	https://www.maxquant.org/archive/maxquant
Proteome Discoverer (v 2.4.1.15)	Thermo Scientific	https://www.thermofisher.com/tw/zt/home/industrial/mass-spectrometry/liquid-chromatography-mass-spectrometry-lc-ms/lc-ms-software/multi-omics-data-analysis/proteome-discoverer-software.html
Mascot search engine (v.2.7.0)	Matrix Science	https://mascot.biotech.illinois.edu/mascot/index.html
targetlynx™ 4.0 software	Waters Corp.	https://waters-targetlynx.software.informer.com/4.0/

(*Continued on next page*)

Please cite this article in press as: Chou et al., PAICS ubiquitination recruits UBAP2 to trigger phase separation for purinosome assembly, Molecular Cell (2023), https://doi.org/10.1016/j.molcel.2023.09.028

Continued

REAGENT or RESOURCE	SOURCE	IDENTIFIER
Spectra Analysis software (v2.15.02)	Jasco	https://jascoinc.com/products/spectroscopy/spectroscopy-software/
Agilent LC/MS Data Acquisition software 9.0	Agilent	https://www.agilent.com/
Agilent Qualitative Analysis 10.0	Agilent	https://www.agilent.com/
Agilent Profinder 10.0	Agilent	https://www.agilent.com/

RESOURCE AVAILABILITY

Lead contact

Further information and requests for resources and reagents should be directed to and will be fulfilled by the lead contact, Ruey-Hwa Chen (rhchen@gate.sinica.edu.tw).

Materials availability

All unique reagents generated in this study will be available from the lead contact upon request.

Data and code availability

- The original MS data are deposited to the ProteomeXchange Consortium via PRIDE partner repository with the project accession number PXD025298 (for ASB11 interactome, ubiquitylome and proteome data), PXD038411 (for PAICS ubiquitination sites data), and PXD027946 (for PAICS and PAICS K74R interactome data). The original data for blot and confocal are deposited to Mendeley dataset (https://doi.org/10.17632/phgv7p6j5k.4). The metabolomics data are deposited to MetaboLights with the project accession number MTBLS8573. All these datasets are publicly available as of the date of publication.
- This paper does not report original code.
- Any additional information required to reanalyze the data reported in this paper is available from the lead contact upon request.

EXPERIMENTAL MODEL AND STUDY PARTICIPANT DETAILS

E. coli strains

BL21 (DE3) and Rosetta2 (DE3) cells were used in this study for the production of recombinant proteins.

Mammalian cell culture and transfection

293T, 293FT, and HeLa cells were obtained from ATCC and cultured in Dulbecco's modified Eagle's medium (DMEM) supplemented with 10% fetal bovine serum (FBS) and 1% penicillin-streptomycin (Pen-Strep). C2C12 cells were provided by Ya-Wen Liu (National Taiwan University, Taipei, Taiwan) and cultured in DMEM supplemented with 10% FBS, 1 mM sodium pyruvate, 2 mM L-glutamine, and 1% Pen-Strep. Melanoma cell lines A375, A2058, and WM115 were provided by Che-Hung Shen (National Health Research Institutes, Tainan, Taiwan) and cultured in RPMI-1640 medium supplemented with 10% FBS and 1% Pen-Strep. PDM treatment was performed as previously described[3] by replacing FBS in the culture medium with dialyzed FBS (Gibco). The following compounds were supplemented to the culture medium as needed: 84 μg/ml arginine-HCl, 100 μM MMF, or 100 μM Inosine. All cells were maintained in a 37°C incubator with a humidified 5% CO_2 atmosphere. Transient transfection of 293T and 293FT cells was performed by calcium phosphate method, whereas HeLa and A375 cells were transfected by lipofectamine 2000 reagent (Invitrogen).

Mice

7-week-old or 8-week-old male NOD/SCID (NOD.CB17-*Prkdc*^{scid}/NcrCrlBltw) mice from BioLASCO Co., Taiwan, were used in this study. All mouse experiments were conducted with the approval from the Institutional Animal Care and Use Committee, Academia Sinica, Taipei, Taiwan.

METHOD DETAILS

Plasmids

Mammalian and baculovirus expression constructs

Plasmids encoding Myc-ASB11, Myc-ASB11ΔSOCS, HA-ElonginB, T7-ElonginC, V5-ROC2, and Myc-Cul5 were described previously.[41] ASB11 cDNA was subcloned to pmcherry-N1. Plasmids encoding His-Ub WT, KR, and K-only mutants were described previously.[58] RFP-Ub was a gift from Wei Yuan Yang (Academia Sinica, Taipei, Taiwan). Plasmids for 3xHA-TurboID-NLS_pCDNA3 (#107171), pPAICS-EGFP (#99108), pFGAMS-mEos2 (#105128), and ADSL-EGFP (#99109) were purchased from Addgene. All

Please cite this article in press as: Chou et al., PAICS ubiquitination recruits UBAP2 to trigger phase separation for purinosome assembly, Molecular Cell (2023), https://doi.org/10.1016/j.molcel.2023.09.028

PAICS K/R mutants were generated by site-directed mutagenesis. The cDNAs for PAICS WT and K74R were subcloned to pRK5-Flag and pAS4.1w.Pbsd-aOn. The cDNA for PAICS was subcloned to pmcherry-N1. The cDNAs for ASB11ΔSOCS, PAICS, and PAICS K74R were subcloned to the *EcoRI-XhoI* sites of 3xHA-TurboID-NLS_pCDNA3, thus generating fusion proteins without the NLS fragment. Construct for UBAP2 (#RG211506) was purchased from ORIGENE and was subcloned to pRK5-Myc and pmcherry-N1. All UBAP2 internal deletion constructs were generated by Q5 Site-directed Mutagenesis Kit (Biolabs, #E05543) and cloned to pRK5-Myc, whereas ΔUBA (Δ48-92), ΔIDR (Δ130-1119), and Δ(982-1119) mutants were generated by PCR and cloned to pRK5-Myc. The cDNAs for UBAP2 WT and ΔUBA were subcloned to pAS4.1w.Pbsd-aOn for inducible overexpression. The cDNAs for Myc-UBAP2 and Myc-UBAP2ΔUBA were subcloned to pVL1392 for generating recombinant proteins in baculovirus. To generate construct for UBAP2 UBA^R, the UBA1/2 domain of USP5 (amino acids 654 to 762) was PCR amplified from USP5 cDNA, a gift from Guang-Chao Chen (Academia Sinica, Taipei, Taiwan), and subcloned to the N-terminus of UBAP2ΔUBA construct.

E. coli *expression constructs*

pMCSG17-NleL (#66716) was purchased from Addgene. The cDNA for Ub K48R with an additional N-terminal Cys residue was cloned to pRSFDuet-1. The cDNAs for PAICS WT and PAICS K74R were cloned to pPET-28b, whereas UBAP2Δ130-621, UBAP2-ΔUBA, and UBAP2ΔIDR were cloned to pPET-28a. UBAP2 UBA domain (amino acids 46-94) was PCR amplified and subcloned pRSFDuet-1-8X His-MBP.

Lentiviral production and infection

Lentiviruses were generated by transfection of packaging plasmid (pCMVΔ8.91), envelope VSV-G plasmid (pMD.G), and various shRNA or cDNA expression constructs into 293FT cells. One day after transfection, the supernatant was filtered through a 0.45 μm filter. For infection, the viral stock was supplemented with 8 μg/ml polybrene and the infected cells were selected with 1 μg/ml puromycin or blasticidin.

RT-qPCR

Total mRNAs were isolated from cells by TRIZOL reagent (Invitrogen) and were reverse transcribed by iScript™ cDNA Synthesis Kit (Bio-Rad). RT-qPCR was performed by FastStart Universal SYBR Green Master reagent (Roche). Amplification was performed on a Light Cycler® 480 instrument II system (Roche) and GAPDH was used as an internal control. Primer sequences are listed in Table S5.

RNA interference

Lentivirus-based shRNA constructs were obtained from National RNAi Core Facility (Taiwan). The DNA fragments for expressing shASB11 and shUBAP2 were subcloned to pLASw.3xLacO-M2 for inducible knockdown. siRNAs were purchased from Horizon Discovery. The target sequences of shRNAs and siRNAs are listed in Table S5.

Immunoprecipitation

Cells were lysed with RIPA buffer containing 50 mM Tris (pH 8.0), 0.15 M NaCl, 1% NP40, 1% sodium deoxycholate, 0.1% SDS, 1 mM PMSF, 1 μg/ml aprotinin, and 1 μg/ml leupeptin. The cell lysates were incubated with primary antibody for overnight, followed by incubating with the Pure Proteome Protein A/G Magnetic Beads (LSK MANGA/G10, EMD Millipore) for 1.5 h. The beads were washed with RIPA buffer and the bound proteins were analyzed by Western blot.

In vivo ubiquitination assay

Cells transfected with His-Ub and other constructs were treated with 1 μM MG132 for 16 h and lysed under denaturing conditions by buffer A [6 M guanidine-HCl, 0.1 M Na_2HPO_4/NaH_2PO_4 (pH 8.0), and 10 mM imidazole]. Cell lysates were incubated with Ni-NTA Sepharose beads for 2 h at 4°C. The beads were washed once with buffer A, twice with buffer A/TI (1 vol buffer A: 3 vol buffer TI [25 mM Tris-HCl pH 6.8, and 20 mM imidazole]), and three times with buffer TI, followed by Western blot analysis. In all experiments, equal expression of His-Ub was verified by Western blot.

In vitro ubiquitination assay

ASB11-based Cul5 E3 ligase complex was purified using anti-Flag M2 affinity agarose beads (Sigma) from lysates of 293T cells transfected with Flag-ASB11, Myc-Cul5, V5-ROC2, T7-ElonginC, and HA-ElonginB. Additionally, Flag-PAICS was purified from transfected 293T cells by M2 beads (Sigma-Aldrich) and eluted using the Flag Peptide elution buffer [5 mg/ml Flag Peptide (Sigma-Aldrich), 50 mM Tris-HCl pH 7.4, 150 mM NaCl]. The E3 ligase complex bound on beads was incubated in a 20 μl reaction mix containing E1, E2 (UbcH5a), His-Ub, and Flag-PAICS as described previously.[41] All reagents used in this assay were purchased from R&D Systems.

In vitro deubiquitination by USP30

The ubiquitinated PAICS was purified using anti-Flag M2 affinity magnetic beads from lysates of 293T cells transfected with Myc-ASB11, His-Ub, and Flag-PAICS. For in vitro deubiquitination assay, the purified ubiquitinated PAICS was incubated in a reaction mix containing 0.17 μM purified USP30 (a gift from Yane-Shih Wang, Institute of Biological Chemistry, Academia Sinica, Taipei, Taiwan), 50 mM Tris (pH 8.0), and 10 mM DTT at 37 °C for overnight.

Please cite this article in press as: Chou et al., PAICS ubiquitination recruits UBAP2 to trigger phase separation for purinosome assembly, Molecular Cell (2023), https://doi.org/10.1016/j.molcel.2023.09.028

Baculovirus protein expression and purification

Sf21 cells were cultured with ESF 921 insect cell culture medium (Expression Systems) containing 10% FBS at 27°C for 2 h. The cells were transiently transfected with 0.5 μg BestBac DNA (Expression Systems) and 2 μg pVL1392-based construct by the Expres2TR transfection reagent (Expression Systems). The transfected cells were cultured at 27°C for 5 days to generate recombinant baculovirus. To amplify the viruses, the culture medium was centrifuged at 2000 ×*g* for 5 min and the supernatant was used for infecting a new batch of Sf21 cells. For purification of recombinant Myc-tagged proteins, the infected cells were lysed by RIPA buffer and lysates were incubated with anti-c-Myc magnetic beads (Thermo Scientific) for overnight at 4°C. Then, the beads were washed with RIPA buffer for 3 times, and stored at 4°C in a buffer containing 50 mM Tris-HCl (pH 7.4) and 150 mM NaCl.

Purinosome induction and detection by fluorescence microscopy

Purinosome induction in HeLa cells were conducted by treatment with PDM, 10 μM DMAT, or 10 μM antimycin A for 16 h or 10 μM SHIN1 for 48 h. Next, cells were washed by 1× phosphate-buffered saline (PBS) twice and fixed with 4% formaldehyde at room temperature for 20 min. Subsequently, cells were washed by 1× PBS for 3 times, and blocked by blocking buffer (1% BSA and 10% goat serum in 1× PBS) with DAPI (Sigma-Aldrich) at room temperature for at least 20 min. The cells were washed by 1× PBS for 3 × 5 min, and mounted onto slides using fluorescence mounting medium (Dako). Next, cells were examined by a confocal microscope (Olympus, FV3000) with a 60x oil objective lens (Olympus Objective Lens, UPlanXApo, 60x/1.42 Oil, ∞/0.17/OFN26.5) and images were collected by Olympus FV3000 FV31S-SW (v 2.40) software.

Quantification of puncta number and colocalization

For analyzing puncta numbers, cell images were thresholded and processed by the Analyzed Particles function in ImageJ. Puncta with a size larger than 0.05 μm^2 were counted. For each biological repeat, at least 30 cells were analyzed in each group and the average number of puncta/cell was quantified. To quantify the colocalization of puncta, images in one channel were thresholded and underwent particle identification by the Analyzed Particles function in ImageJ. Then, the same parameters were used to analyze the images in another channel for calculating the colocalized puncta. The number of biological repeats and number of cells scored in each repeat are the same as puncta quantification.

Time-lapse fluorescence imaging

Time-lapse imaging was performed at 37°C under 5% CO_2 atmosphere using a confocal microscope (Olympus, FV3000) equipped with a 60x oil objective lens (Olympus Objective Lens, UPlanXApo, 60x/1.42 Oil, ∞/0.17/OFN26.5). The images were acquired with a 5 s interval for 30 captures by an Olympus FV3000 FV31S-SW (v 2.40) software and processed by ImageJ.

PLA

PLA was assayed by Duolink® Proximity Ligation Assay Kit (Sigma-Aldrich) according to the manufacturer's instructions. Briefly, cells were fixed with 4% formaldehyde. After washed 3 times by 1× PBS, cells were permeabilized with ice-cold methanol at 4°C for 10 min and washed with 1× PBS. Cells were blocked by Duolink Blocking Solution at room temperature for 1 h and then incubated with primary antibodies at 4°C for overnight. Next, cells were washed in wash buffer A for 2 × 5 min and then incubated with PLA probes at 37°C for 1 h. After washing in wash buffer A for 2 × 5 min, cells were incubated with ligation solution at 37°C for 1 h and washed in wash buffer A for 2 × 2 min. Cells were then incubated with Amplification-Polymerase solution at 37°C for 100 min and washed in wash buffer B for 2 × 10 min. The coverslips were mounted onto slides using a mounting buffer with DAPI and examined by confocal microscopy as described above.

ChIP and Re-ChIP assays

ChIP analysis was performed as previously described[59] with slight modifications. Briefly, cells were treated with 1% formaldehyde for 10 min to cross-link the chromatins followed by quenched with 125 mM glycine for 5 min. Cells were lysed by ChIP lysis buffer (15 mM HEPES pH 7.5, 140 mM NaCl, 1 mM EDTA, 0.5 mM EGTA, 1% Triton X-100, 0.1% sodium deoxycholate, 0.1% SDS, 0.5% sodium lauroylsarcosine) with protease inhibitors. The lysates were sonicated and then centrifuged. Proteins in the supernatants were quantified by Bradford reagent. Lysates containing 0.7 mg proteins were pre-cleared by protein A magnetic beads (Millipore) for 1 h at 4°C and then incubated with ChIP level antibody at 4 °C for overnight, followed by incubating with 50 μl protein A magnetic beads for 1 h at 4°C. Beads were washed 5 times with ChIP buffer (50 mM HEPES pH 7.5, 1 mM EDTA, 1% NP40, 0.5M LiCl, 0.7% sodium deoxycholate, and protease inhibitors) and 1 time with TE wash buffer (10 mM Tris pH 8.0, 1 mM EDTA, and 50 mM NaCl). Next, the protein-DNA complexes were eluted by elution buffer (TE buffer with 0.25 M NaCl and 0.5% SDS) at 65 °C for 20 min. For experiments involving Re-ChIP, the eluent was diluted with TE wash buffer to make the SDS concentration down to 0.1%, followed by incubation with antibody and protein A magnetic beads and the wash and elution steps. For both ChIP and Re-ChIP, the eluents were treated with 250 μg/ml RNase A (Thermo) for 5 min at 37 °C and DNA was extracted by QIAamp DNA Mini Kit (QIAGEN) and analyzed by qPCR.

Please cite this article in press as: Chou et al., PAICS ubiquitination recruits UBAP2 to trigger phase separation for purinosome assembly, Molecular Cell (2023), https://doi.org/10.1016/j.molcel.2023.09.028

Quantitative ubiquitylome and proteome analyses by SILAC labeling and LC-MS/MS

SILAC-labeling

Cells were cultured in SILAC medium containing DMEM deficient in L-arginine and L-lysine (Thermo), 10% dialyzed FBS (Biological Industries), Pen-Strep, and L-arginine-HCl [$^{13}C_6$, $^{15}N_4$] (Arg-10) together with L-lysine-HCl [$^{13}C_6$] (Lys-6) (Thermo), or L-arginine (Arg-0) together with L-lysine (Lys-0) (Thermo), respectively, for 2 weeks. Cells were then treated with 1 μM MG132 for 16 h, washed twice with ice-cold PBS, and harvested.

Sample preparation

Cell pellets were lysed at room temperature in urea lysis buffer containing 9 M urea, 20 mM HEPES (pH 8.0), and protease inhibitor (Roche). The lysates were cleared by centrifugation at 15000 rpm for 10 min. Braford assay was used to determine the protein concentration. Lysates with equal amounts of proteins but different SILAC labeling were combined. Proteins were reduced with 5 mM DTT (Sigma-Aldrich) at 37°C for 70 min and alkylated with 10 mM iodoacetamide (Sigma-Aldrich) at room temperature for 60 min. Lysates were diluted to 4 M urea with 20 mM HEPES (pH 8.0) and digested with Lys-C (Wako) at 37°C for 4 h. The peptide mixtures were diluted to 1.5 M urea and subsequently digested with Trypsin (Promega) at 37°C for overnight. The reaction was quenched with trifluoroacetic acid (TFA) and the peptide solutions were centrifuged, desalted using a Sep-Pak PlusC18 cartridge (Waters), and lyophilized.

Fractionation

Peptides for proteome analysis were fractionated before LC-MS/MS. Fractionation was performed with Pierce High pH Reversed-Phase Peptide Fractionation Kit (Thermo) according to the manufacturer's instruction. Briefly, peptides were reconstituted in 0.1% TFA and loaded onto an equilibrated, high-pH, reversed-phase fractionation spin column. Peptides were bound to the hydrophobic resin under aqueous conditions and desalted by washing the column with water. Bound peptides were eluted into eight fractions and collected by centrifugation with a step gradient of increasing acetonitrile (ACN) concentration.

K-ε-GG peptide enrichment

Enrichment was performed with anti-K-ε-GG antibody from the PTMScan Ubiquitin Remnant Motif (K-ε-GG) Kit (Cell Signaling Technology) with procedures described previously.[60] The enriched peptides were subjected to ubiquitylome analysis by NanoLC−nanoESI-MS/MS performed on a Thermo UltiMate 3000 RSLCnano system connected to an Thermo Orbitrap Fusion mass spectrometer (Thermo Fisher Scientific) equipped with a nanospray interface (New Objective). Peptide mixtures were loaded onto a 75 μm ID, 25 cm length PepMap C18 column (Thermo Fisher Scientific) packed with 2 μm particles with a pore width of 100 Å and were separated using a segmented gradient in 120 min from 5% to 35% solvent B (0.1% formic acid in ACN) at a flow rate of 300 nl/min. Solvent A was 0.1% formic acid in water. The mass spectrometer was operated in the data-dependent mode. Briefly, survey scans of peptide precursors from 350 to 1600 m/z were performed at 120K resolution with a 2×10^5 ion count target. Tandem MS was performed by isolation window at 1.6 Da with the quadrupole, HCD fragmentation with normalized collision energy of 30, and MS^2 scan analysis at 30K resolution in the orbitrap. The MS^2 ion count target was set to 5×10^4 and the max injection time was 54 ms. Only those precursors with charge state 2-6 were sampled for MS^2. The instrument was run in top speed mode with 3 s cycles; the dynamic exclusion duration was set to 15 s with a 10 ppm tolerance around the selected precursor and its isotopes. Monoisotopic precursor selection was turned on.

Proteome analysis

NanoLC−nanoESI-MS/MS analysis was performed on a nanoAcquity system (Waters) connected to the Orbitrap Elite hybrid mass spectrometer (Thermo Electron) equipped with a PicoView nanospray interface (New Objective). Peptide mixtures were loaded onto a C18 BEH column (Waters) packed with 1.7 μm particles with a pore width of 130 Å and were separated using a segmented gradient in 90 min from 5% to 35% solvent B at a flow rate of 300 nl/min and a column temperature of 35°C. The mass spectrometer was operated in the data-dependent mode. Briefly, survey full scan MS spectra were acquired in the orbitrap (*m/z* 350–1600) with the resolution set to 120K at *m/z* 400 and automatic gain control (AGC) target at 10^6. The 20 most intense ions were sequentially isolated for CID MS/MS fragmentation and detection in the linear ion trap (AGC target at 10000) with previously selected ions dynamically excluded for 60 s. Ions with singly and unrecognized charge state were also excluded.

Database search

Peptides were identified with MaxQuant search engine (v1.6.17.0). The database was downloaded from Uniprot and consists of 20187 human target sequences. The enzyme specificity was set to trypsin (full) allowing for two missed cleavages and precursor mass tolerances were 10 ppm for parent ions and 0.2 Da for fragment ions. Dynamic modifications were set for heavy lysine ($^{13}C_6$) (+ 6.02013), heavy arginine ($^{13}C_6{}^{15}N_4$) (+ 10.00827), lysine ubiquitination (+114.04293 Da/+383.22810) (heavy amino acids and lysine-ε-GG were only set for SILAC experiment), methionine oxidation (+15.99492 Da), asparagine and glutamine deamidation (+0.98402 Da) and protein N-terminal acetylation (+42.03670). A maximum of 3 dynamic modifications was allowed per peptide and a static modification of +57.02147 Da was set for carbamidomethyl cysteine.

Proximity biotinylation by TurboID

HeLa cells transfected with HA-TurboID-based constructs were treated with 500 μM biotin for 24 h. Cells were lysed by TurboID lysis buffer (50 mM Tris pH 7.4, 500 mM NaCl, 0.4% SDS, 5 mM EDTA, 1 mM DTT, 2% Triton X-100, 1 mM PMSF, 1 μg/ml aprotinin, and 1 μg/ml leupeptin). Cell lysates were incubated with MyOne Streptavidin C1 Dynabeads (Invitrogen) at 4 °C for overnight. Beads were washed sequentially with wash buffer 1 (50 mM Tris pH 7.4, 500 mM NaCl, 2% SDS, 5 mM EDTA) for one time, wash buffer 2 (0.2%

Please cite this article in press as: Chou et al., PAICS ubiquitination recruits UBAP2 to trigger phase separation for purinosome assembly, Molecular Cell (2023), https://doi.org/10.1016/j.molcel.2023.09.028

deoxycholate, 1% Triton X-100, 500 mM NaCl, 1 mM EDTA, and 50 mM HEPES pH 7.5) for one time, wash buffer 3 (250 mM LiCl, 0.5% NP-40, 0.5% deoxycholate, 1% Triton X-100, 500 mM NaCl, 1 mM EDTA, and 10 mM Tris pH 8.1) for one time, and wash buffer 4 (50 mM Tris pH 7.4 and 50 mM NaCl) for two times. The bound proteins were analyzed by label-free quantitative LC-MS/MS.

Label-free quantitative LC-MS/MS analysis

NanoLC–nanoESI-MS/MS analysis was performed on a nanoAcquity system (Waters) connected to the LTQ Orbitrap Velos hybrid mass spectrometer (Thermo Electron) equipped with a PicoView nanospray interface (New Objective). The operation was followed the procedures described in the proteome analysis above. Peptide identification was performed using the percolator node within Proteome Discoverer (v 2.4.1.15; Thermo Scientific) against the Swiss-Prot Human database (561,911 entries total). Search criteria used were trypsin digestion, variable modifications set as carbamidomethyl (C), oxidation (M), ubiquitination (K) allowing up to two missed cleavages, mass accuracy of 10 ppm for the parent ion and 0.02 Da for the fragment ions. The false discovery rate (FDR) was set to 1% for peptide identifications. For label-free quantification, precursor ions intensities were extracted using Minora Feature Detector node in Proteome Discoverer with a 2 ppm mass precision and 2 min retention time shift (align the LC/MS peaks mapping to the isotope pattern and retention time).

Determination of ubiquitination sites by LC-MS/MS

The ubiquitinated PAICS was isolated from 293T cells transfected with His-Ub, Myc-ASB11, and Flag-PAICS using anti-Flag M2 affinity agarose (Sigma-Aldrich). The immunoprecipitated proteins were incubated with Lb^{Pro*} reaction buffer containing 50 mM Tris-HCl (pH 8.0), 10 mM DTT, and 50 μM Lb^{Pro*} at 37 °C for overnight. The reaction mix was separated by SDS-PAGE and stained with SYPROTM Ruby Protein Gel Stain (Invitrogen). The protein band corresponding to the molecular weight of free-form Flag-PAICS was excised for in-gel digestion and MS peptide sequencing. Briefly, gel slices were destained with 50% ACN/25 mM ammonium bicarbonate, reduced by 5 mM dithioerythritol, and alkylated by adding 10 mM iodoacetamide. Gel slices were then washed four times with 50% ACN/25 mM ammonium bicarbonate and dried by soaking in 100% ACN. After evaporating ACN, proteins were digested with Lys-C (Wako) at 37 °C for 3 h and then with trypsin (Promega) at 37 °C for 18 h. Next, peptides were extracted by adding 50% ACN/5% TFA. The supernatant was desalted by Zip-Tip and lyophilized. LC-MS/MS analysis was performed with conditions as described in proteome analysis.

Peptide identification was performed using Mascot search engine (v.2.7.0; Matrix Science) against the Swiss-Prot Human database (561,911 entries total). Search criteria and FDR were as described in label-free LC-MS/MS. Peptide sequence assignments contained in MASCOT search results were validated by manual confirmation from raw MS/MS data.

Metabolite profiling analysis

Cells were extracted with 80% methanol at -80 °C for 15 min. Cell lysates were centrifuged and the supernatants were dried by SpeedVac and stored at -80°C. The dry samples were dissolved in ddH2O and were centrifuged at 12,000 ×*g* for 30 min to remove debris. The supernatant was analyzed with Waters Acquity UPLC-TQXS (Waters) by a previously described method.[61] Chromatographic separation was performed on a Waters ACQUITY BEH C18 column (2.1 mm × 100 mm × 1.7 μm) at 45 °C and with elute A (water with 10 mM tributylamine and 15 mM acetic acid) and elute B (50% ACN with 10 mM tributylamine and 15 mM acetic acid). The gradient profile was as follows: keep 4% B, 6 min; linear gradient 4-50% B, 0.1 min; 50%- 60% B, 2.9 min; 60-100% B, 0.8 min, and keep 2.2 min. The column was then re-equilibrated for 3 min. Mass was operated in negative mode and positive mode with multiple reaction monitoring. The parameters were as follows in both positive and negative modes: desolvation temperature was set at 500 °C capillary 1000 V; source temperature was set at 150°C; desolvation gas flow was set at 1000 L/h.

For methionine cycle-related metabolites analysis, an HSS T3 column (2.1 mm × 100 mm × 1.8 μm) was used for chromatographic separation with elute A (water with 0.1% formic acid) and elute B (ACN with 0.1% formic acid) by a previous method.[62] Briefly, the gradient profile was as follows: 0% B, 2 min; linear gradient 0-40% B, 3 min; 40-98% B, 2 min. The mass was operated in positive mode. The desolvation temperature and source temperature were 600°C and 150°C, respectively. The result was analyzed using the targetlynx™ 4.0 software (Waters).

Isotope labeling and metabolic flux assay

Cells were treated with antimycin A or DMAT for 12 h and then labeled with 10 mM $^{13}C_6$-glucose (Cambridge Isotope Laboratories, Inc.) in the presence of antimycin A or DMAT for 14 h. Cells were extracted with 40% methanol/40% ACN in ddH_2O at -80 °C for 15 min. Cell lysates were centrifuged and the supernatants were dried by SpeedVac and stored at -80°C. The dry samples were dissolved in ddH_2O and were centrifuged at 12,000 ×*g* for 30 min to remove debris. The supernatants were analyzed on an Agilent 1290 II Infinity Ultra-High-Performance Liquid Chromatography system (Agilent Technologies) with an Agilent 6545XT quadrupole time-of-flight (Q-TOF) mass spectrometer (Agilent Technologies). The sample was separated using ACQUITY UPLC BEH amide column (2.1 mm × 100 mm × 1.8 μm, Waters) at 40°C. The mobile phases were composed of deionized water (eluent A) and LC-MS grade 90% (v/v) ACN (Sigma Aldrich) (eluent B), both eluent with 15 mM ammonium acetate and 0.3% $NH_3 \cdot H_2O$. The flow rate was 300 ul/min and the injection volume of sample was 5 ul. The mass spectrometer was equipped with an Agilent Jet-stream source operating in positive and negative full-scan ion mode collected from m/z of 50-1500. The chromatogram acquisition, detection of mass spectral peaks, and their waveform processing were performed using Agilent LC/MS Data Acquisition software 9.0 and Agilent Qualitative

Please cite this article in press as: Chou et al., PAICS ubiquitination recruits UBAP2 to trigger phase separation for purinosome assembly, Molecular Cell (2023), https://doi.org/10.1016/j.molcel.2023.09.028

Analysis 10.0 (Agilent, USA). Isotopologue extraction was performed and natural isotope abundance was corrected using Agilent Profinder 10.0 (Agilent). The mass tolerance was set to ±10 ppm and retention time tolerance was ±0.5 min in isotopologue extraction parameters.

Alternatively, cells treated with antimycin A or DMAT were pulse labeled with 10 mM $^{13}C_6$-glucose (Cambridge Isotope Laboratories, Inc.) for 5 min. Metabolite extraction and analysis were followed the procedures as described in metabolite profiling analysis.

Gene editing by CRISPR

For targeted knockout of UBAP2 expression, a gRNA (5'- GAGCAACTGCAAGTAGTAAG-3') designed to target the upstream intron of UBAP2 translation start site was cloned into the *BsmBI* sites of an all-in-one CRISPR/Cas9 expression vector (provided by National RNAi Core Facility, Taipei, Taiwan). HeLa cells were transfected with plasmids encoding Cas9/gRNA by using Lipofectamine 3000 (Invitrogen). Two days after transfection, cells were treated with 1 μg/ml of puromycin for 48 h. Single cell-derived colonies were established through the limiting dilution method and knockout efficiency was examined by Western blot.

For targeted knock-in of GFP_{11} fragment, a gRNA (5'-CCCTAAAAAATTCAATGGCA-3') designed to target the 3'end of PAICS coding sequence was cloned into the *BsmBI* sites of an all-in-one CRISPR/LbCpf expression vector (provided by National RNAi Core Facility). A synthetic donor (ssODN) template (5'-CAAGCATTTTGAACACATGGATTTCCTTGAAGCAGGCTGACAAGAAAATCAGAG AATGTAATTTAtccggtggcggtggcagc**CGTGACCACATGGTCCTTCATGAGTATGTAAATGCTGCTGGGATTACATAA**GAAAGAA TGCCATTGAATTTTTTAGGG**GAGAA**AACTACAAATTTCTAATTTAGCTGAAGGAAAATC; PAICS homologous arms [uppercase], GS-linker [lowercase], GFP_{11} fragment and stop codon [bold], gRNA targeting sequences [underline] and PAM sequence [italic]) encoding the GS-linker-GFP_{11} fragment and homologous arms was synthesized by Integrated DNA Technologies. Of note, a single nucleotide insertion (italic, underline) was introduced to disrupt the PAM sequence of ODN donor for enhancing the GFP_{11} knock-in frequency. To enhance the homologous recombination frequency, HeLa cells were synchronized by double-thymidine block before transfection. In brief, cells were grown in the presence of 2 mM thymidine for 12-14 h, released by culturing in thymidine-free medium for 8-9 h and then grown again for 12-14 h with 2 mM thymidine. For the final release from G1 arrest, HeLa cells were replaced with fresh medium supplemented with 200 nM KU0060648 and 1 mM VPA. Transfection was carried out with plasmid encoding Cpf1/gRNA and GFP_{11} donor ODN by using Lipofectamine 3000 (Invitrogen). After treatment with 1 μg/ml of puromycin for 48 h, cells were re-transfected with plasmid encoding GFP_{1-10} reporter (Addgene #80409). Cells displaying green fluorescence were collected by cell sorter and single cell-derived colonies were established by limiting dilution method.

Fumarate assay

Cellular concentration of fumarate was assayed by fumarate assay kit (Sigma-Aldrich) according to the manufacturer's instructions. Briefly, cells were lysed in fumarate assay buffer and centrifuged at 13,000 ×*g* for 10 min. The supernatant (50 μl) was added to a 96-well plate, followed by adding 100 μl of master reaction mix and incubated for 30 min at room temperature before absorbance measurement at 450 nm. The concentrations of fumarate were calculated by a fumarate standard curve.

PAICS activity assay

The SAICARs activity of PAICS was assayed as described previously.[63] Briefly, equal amounts of purified PAICS and PAICS K74R were incubated with 180 mM L-aspartate (Sigma Aldrich), 10 mM CAIR, and 30 mM ultrapure ATP in the PAICS assay buffer (50 mM Tris-HCl pH 8.0, 10 mM DTT, 0.01% BSA, 0.01% Tween 20, 20 mM $MgCl_2$) for 40 min at room temperature. ADP generated from the reaction was quantified by ADP-Glo Kinase Assay Kit (Promega) according to the manufacturer's instructions. Controls in which PAICS/PAICS K74R or L-aspartate/ATP were replaced with PAICS assay buffer were included. The luminescence was measured and ADP concentrations were calculated by an ADP standard curve.

Far-UV CD spectroscopy

PAICS WT and PAICS K74R in a buffer containing 50 mM HEPES pH 7.5, 100 mM NaCl, 5% glycerol, and 10 mM β-ME were measured with a Jasco J-815 spectrometer equipped with a PTC-424S Peltier-type temperature controller (Jasco) in a 0.1 mm path length quartz cell (FireflySci). Far-UV spectra were collected at 25°C in a continuous scanning method from 195 to 260 nm, a 0.5 nm data pitch, a 1 nm spectral bandwidth, a 4 s data integration time, a 10 nm/min scanning speed, and 3 accumulation cycles. All spectra were buffer-subtracted and smoothened by using the Spectra Analysis Software (version 2.15.02, Jasco).

Protein expression and purification

Expression and purification of Lb^{Pro*} were described previously.[57]

His-Cys-Ub K48R, His-UBAP2Δ130-621, His-UBAP2ΔIDR, His-UBAP2Δ130-621/ΔUBA, UBAP2 UBA, and GST-NleL were expressed in Rosetta2 (DE3), whereas His-PAICS and His-PAICS K74R were expressed in BL21 (DE3). Bacteria were grown in LB media to OD_{600} of 0.6-0.8 and then recombinant protein expression was induced by culturing in 0.5 mM IPTG at 16-18 °C for 18-20 h. The cultures were centrifuged to collect bacteria pellet for protein purification.

For purifying His-UBAP2ΔIDR, His-PAICS, and His-PAICS K74R from soluble fraction of lysates, bacteria pellet was re-suspended in His-lysis buffer (50 mM HEPES pH 7.5, 500 mM NaCl, 10% glycerol, 20 mM imidazole, 10 mM β-ME, 1 mM PMSF) and lysed by sonication. The lysate was cleared by centrifugation and the supernatant was loaded onto a column containing Ni-NTA Sepharose

Please cite this article in press as: Chou et al., PAICS ubiquitination recruits UBAP2 to trigger phase separation for purinosome assembly, Molecular Cell (2023), https://doi.org/10.1016/j.molcel.2023.09.028

resin (GE Healthcare Life Sciences). After washing the column sequentially with His-wash buffer (50 mM HEPES pH 7.5, 150 mM NaCl, 10% glycerol, 10 mM β-ME) supplemented with 20, 50, and 100 mM imidazole, the His-tagged proteins were eluted by His-elution buffer (50 mM HEPES pH 7.5, 150 mM NaCl, 10% glycerol, 500 mM imidazole, 10 mM β-ME). For His-PAICS and His-PAICS K74R, they were further purified by size-exclusion chromatography (SEC) with a Superdex 75 column (Cytiva) and eluted by SEC buffer (50 mM HEPES pH 7.5, 100 mM NaCl, 10 mM β-ME).

For purifying His-MBP-UBAP2 UBA from soluble fraction of lysates, bacteria pellet was re-suspended in lysis buffer containing 50 mM HEPES pH 7.5, 300 mM NaCl, 20 mM imidazole, 10 mM β-ME, and 1 mM PMSF and lysed by sonication. The lysate was cleared by centrifugation and the supernatant was loaded onto a column containing Ni-NTA Sepharose resin (GE Healthcare Life Sciences). After washing the column with a wash buffer containing 50 mM HEPES pH 7.5, 150 mM NaCl, 20 mM imidazole, and 10 mM β-ME, the His-tagged proteins were eluted by elution buffer containing 50 mM HEPES pH 7.5, 150 mM NaCl, 500 mM imidazole, and 10 mM β-ME. The protein was further purified by SEC with a Hiload Superdex 200 column (Cytiva) and eluted by SEC buffer.

For purifying His-Cys-Ub K48R from soluble fraction, bacteria were lysed by sonication in a buffer containing 20 mM HEPES (pH 7.5), 300 mM NaCl, 10 mM imidazole, 10 mM β-ME, 1 mM PMSF and protein was purified by Ni-NTA Sepharose column as described above, except that sequential wash buffers containing 20 mM HEPES (pH 7.5), 300 mM NaCl, 10 mM β-ME, supplemented with 10 mM and 20 mM imidazole and elution buffer containing 20 mM HEPES (pH 7.5), 300 mM NaCl, 600 mM imidazole, and 10 mM β-ME were used. The His tag was then cleaved by adding TEV protease to the eluent (1/50 vol/vol) and dialyzed in dialysis buffer (20 mM HEPES pH 7.5, 300 mM NaCl, 10 mM β-ME) for overnight. The Cys-Ub K48R protein was further purified by SEC with a Superdex 75 column (Cytiva) and eluted by SEC buffer.

For purifying His-UBAP2Δ130-621 and His-UBAP2Δ130-621/ΔUBA from inclusion bodies, bacteria pellet was re-suspended in lysis buffer containing 20 mM Tris-HCl pH 7.5, 300 mM NaCl, 10 mM imidazole, 10 mM β-ME, 1 mM PMSF and lysed by sonication. The lysate was centrifuged and the pellet was re-suspended in denaturing buffer (50 mM Tris pH 7.5, 100 mM NaCl, 8 M urea) and then centrifuged to remove insoluble materials. The supernatant was applied to a Ni-NTA Sepharose column and the column was washed with urea-wash buffer (50 mM Tris-HCl pH 7.5, 300 mM NaCl, 8 M urea, 10 mM imidazole). Proteins were eluted by urea-elution buffer (50 mM Tris pH 7.5, 300 mM NaCl, 8 M urea, 300 mM imidazole). Then, the eluent was dialyzed with renaturing buffer (50 mM Tris pH 7.5, 100 mM NaCl, 10 mM β-ME) supplemented with 1 M urea for 4 h, followed by renaturing buffer supplemented with 0.1 M urea for 4 h, and renaturing buffer without urea for overnight. His-UBAP2Δ130-621 was further purified by SEC with a Superdex 200 increase column (Cytiva) and eluted by SEC buffer.

For purifying GST-NleL, bacteria were lysed by sonication in GST lysis buffer (50 mM Tris-HCl pH 7.5, 150 mM NaCl, 1% Triton X-100, 1 mM DTT, 1 mM PMSF) and lysate was loaded to a column containing Glutathione Sepharose 4B resin (GE Healthcare Life Sciences), followed by washing with PBS and elution with GST-elution buffer (50 mM Tris pH 8.0, 10 mM reduced glutathione, 1 mM DTT). The GST tag was cleaved by adding TEV protease to the eluent (1/50 vol/vol) and dialyzed in 50 mM Tris pH 8.0, 1 mM DTT for overnight. The reaction mixture was passed through the Glutathione Sepharose 4B column and the flow through was collected for recovering NleL.

All purifications were performed at 4 °C. Purified proteins were concentrated using Amicon spin concentrators.

Generation of K6-linked polyUb chain

The purified Cys-Ub K48R was mixed with FM (1:5 mol/mol) to label the thiol group of Cys and the unconjugated FM was removed by a PD-10 desalting columns (Cytiva). The generation of K6-linked polyUb chain was followed a previous study.[48] Briefly, ubiquitination was performed in 20 μl reaction mix by incubating 20 μM FM-labeled or unlabeled Cys-Ub K48R with 250 nM UBE1 (E1; R&D System), 1 μM UbcH7 (E2; ProSpecbio), 1 μM NleL (E3), 10 mM ATP, 10 mM $MgCl_2$, and 40 mM HEPES (pH 7.5) at 37 °C for 30 min. PolyUb chain formation was analyzed by SDS-PAGE followed by iBright Imaging System (Thermo Fisher Scientific).

In vitro phase separation assay

Purified UBAP2Δ130-621 was fluorescently labeled by Alexa Flour 647 Protein Labeling Kit (Invitrogen) according to the manufacturer's instructions. To test phase separation of UBAP2Δ130-621 with K6-linked polyUb chain, purified UBAP2Δ130-621 (unlabeled or 1% Alexa Flour 647 labeled) was added to the ubiquitination reaction mix containing K6-linked polyUb chain (1% FM-labeled) in a buffer containing 50 mM Tris-HCl (pH 7.5), 100 mM NaCl, 1 mM DTT. To test phase separation of UBAP2Δ130-621 with Ub_4 with different linkages, UBAP2Δ130-621 (1% Alexa Flour 647 labeled) was mixed with unlabeled Ub_4 in the aforementioned buffer. All mixtures were incubated at room temperature for 30 min, dropped on the glass slide with sticker, and sandwiched with a 12 mm coverslip. Images were captured by confocal microscopy as described above.

FRAP assay

FRAP experiments were performed using a 100× 1.49NA Plan objective lens attached to an *iLas* multimodal total internal reflection fluorescence (Roper)/spinning disk (CSUX1, Yokogawa) confocal microscope (Ti-E, Nikon) and followed procedures as described.[64] Briefly, the stage temperature was maintained at 37 °C with an airstream incubator (Nevtek) and focus was maintained using the PerfectFocus™ system (Nikon). Photobleach was conducted by 488 nm (for GFP fluorescence) or 561 nm (for mcherry fluorescence) laser and was applied to a single droplet. Images were acquired at 1s intervals before and after photobleaching using an Evolve

Please cite this article in press as: Chou et al., PAICS ubiquitination recruits UBAP2 to trigger phase separation for purinosome assembly, Molecular Cell (2023), https://doi.org/10.1016/j.molcel.2023.09.028

EMCCD camera (Photometrics) with an ~100 nm evanescent filed depth. Images were captured and processed using the Metamorph software.

Biolayer interferometry (BLI) analysis

BLI analysis was performed on the Octet RED96 System (Sartorius) using a high-precision streptavidin SAX biosensor at amber temperature. Various Ub_4 chains at 30 μM were firstly biotinylated using Biotinylation Kit (ThermoFisher) according to the manufacturer's instructions. Biotinylated Ub_4 chains were diluted to ~300 nM using a buffer containing 25 mM HEPES pH 7.5, 200 mM NaCl, 0.1 mg/ml BSA, 0.01% tween20 and was loaded to SAX biosensors. To estimate the range of K_D, multiple samples of UBAP2 UBA domain at 1–150 μM as the analytes were initially titrated to the Ub_4 biosensors. Six to nine concentrations of the UBA domain (3 to 120 μM) were then prepared to collect the BLI sensorgrams with triplicates. The wavelength shifts of steady-state responses of multiple data points were extracted and fitted by a single-site binding system using Octet analysis software to obtain the dissociation constant K_D.

Cell viability and proliferation assays

Cell viability was determined by incubating cells with 0.4 mg/ml methylthiazolyl diphenyl tetrazolium bromide (MTT, Sigma-Aldrich) for 2 h, followed by cell lysis with DMSO and absorbance measurement at 590 nm. Cell proliferation was assayed by BrdU Proliferation Assay Kit (Merck Millipore) according to the manufacturer's instructions.

Animal studies

2×10^5 A375 cells stably expressing various IPTG-inducible shRNAs and/or Dox-inducible rescue cDNAs were orthotopically inoculated into 7-week-old (for ASB11 and UBAP2 experiments) or 8-week-old (for PAICS experiment) male NOD/SCID (NOD.CB17-*Prkdc*^{scid}/NcrCrlBltw) mice (BioLASCO Co., Taiwan). After 7 days for allowing tumor growth, mice were intraperitoneally injected with 100 μl IPTG (10 μg/μl) or sterilized water and/or fed with Dox-containing diets or normal diets. The sizes of tumors were measured every 3 or 4 days, and their volumes were calculated using the equation $mm^3 = 1/2 \times \text{length (mm)} \times (\text{width (mm)})^2$.

QUANTIFICATION AND STATISTICAL ANALYSIS

Statistical analyses were performed by GraphPad Prism 8. Unpaired two-tailed t-test was used for comparison between two groups, whereas one-way or two-way ANOVA was used for multigroup comparisons.